Title

Nanowires for Photovoltaics and Artificial Photosynthesis

Journal

SEMICONDUCTOR NANOWIRES: FROM NEXT-GENERATION ELECTRONICS TO SUSTAINABLE ENERGY, 2015-January(11)

ISSN

2046-0066

Authors

Yang, Peidong
Brittman, Sarah
Liu, Chong

Publication Date

2015

Chapter X

Nanowires for Photovoltaics and Artificial Photosynthesis

Peidong Yang*[a,b,c], Sarah Brittman[a,c], Chong Liu[a,c]

[a]Department of Chemistry and [b]Department of Materials Science and Engineering,
University of California, Berkeley, CA 94720, United States
[c]Materials Sciences Division, Lawrence Berkeley National Laboratory, Berkeley, CA
94720, United States

p_yang@berkeley.edu

Chapter X - Nanowires for Photovoltaics and Artificial Photosynthesis

X.1 Introduction

Electricity and lighting, heating and cooling, computers, cars, planes–the hallmarks of modern life are synonymous with energy consumption.[1, 2] Since much of the world's ever-growing population lives in societies striving to modernize, the world's need for sources of clean and renewable energy is more urgent than ever.[2] Although the sun offers more than enough power to satisfy humanity's appetite for energy, technologies for solar energy conversion remain too costly to compete with fossil fuels on a worldwide scale.[3, 4] Research into new and improved technology is part of the solution, and photovoltaics and artificial photosynthesis are two approaches with much practical potential.[5-7] Photovoltaics converts sunlight into electricity: small installations can power individual homes or solar farms can light up cities. Nevertheless, storing the sun's energy as a fuel to balance out daily fluctuations or for transportation remains an important demand of modern life. Artificial photosynthesis uses photoelectrochemistry to transform sunlight directly into chemical fuels for these applications. Both of these approaches have a promising future as part of the portfolio of renewable energy technologies that will be needed to wean the world from its dependence on fossil fuels.[6] For this breakthrough to occur, however, these technologies will need to be more efficient and less costly, two challenges that nanowires can help overcome.

The potential of nanowires in solar energy applications lies in their tunable geometric effects and high surface-to-volume ratio. Since the nanowires typically employed in photovoltaic (PV) and photoelectrochemical (PEC) cells are too large to show quantum confinement effects, conventional semiconductor physics applies. In comparison with planar devices, however, they offer a much larger surface-to-volume ratio, with roughness factors reaching up to ~300.[8, 9] Because the dimensions of the nanowires are on the same scale as the wavelength of visible light and the minority carrier diffusion lengths in many solar materials, their geometry can improve light absorption and charge collection in energy conversion devices. Additionally, the high surface-to-volume ratio of nanowires is especially useful for artificial photosynthesis because it increases the surface area available for the fuel-producing chemical reactions. For all these reasons, the unique properties of nanowires make them promising candidates for efficient PV and PEC devices.

This chapter has been organized to emphasize some of the commonalities between photovoltaics and artificial photosynthesis, the contributions that nanowires can make to each field, and the evolution of these contributions. After a brief introduction to each field in sections 2 and 3, section 4 presents some advantages of nanowire devices for solar energy conversion that are common to both fields; the following two sections then address topics that are specific to the individual fields. Section 7 then offers a history of the Yang Group's work in photovoltaics and artificial photosynthesis as a case study of their development over the past eight years. This perspective on the past offers lessons for future achievement in nanowire photovoltaics and artificial photosynthesis, and lastly, section 8 highlights some of the challenges still to be addressed in using nanowires for solar energy conversion.

X.2 Principles of Photovoltaics

Photovoltaics is the conversion of sunlight into electricity using solar cells. In conventional semiconductor solar cells, a *p*-*n* junction establishes a built-in electric field within the material[10, 11] (Fig. X.1a). At the contact interface between the *p*-type and *n*-type semiconductors, excess holes and electrons recombine until the chemical potential difference is counterbalanced by an electrical potential difference. The extent of the area devoid of carriers, or depletion region, depends upon the doping levels of the two sides of junction and the materials' dielectric constants. When a semiconductor absorbs photons, electrons are excited from its valence band to conduction band, producing an electron-hole pair. The built-in electric field at the junction, or band-bending, separates the electron and hole and accelerates them toward the solar cell's contacts to be collected as current. This current and the built-in field's voltage transform the sun's energy into electrical energy. If the photogenerated carriers originate in the semiconductor far from the *p*-*n* junction, the minority carriers must diffuse to the depletion region to be separated. Recombination during this diffusion process and recombination within the depletion region are two of the main loss mechanisms that reduce a solar cell's efficiency.

[Figure X.1 near here]

Several metrics are used to evaluate and compare the performance of solar cells. The current-voltage (*I*-*V)* curve is measured under illumination from a solar simulator, which is a light source that produces 1-sun intensity (100 mW/cm^2) with an AM1.5G spectral profile (Fig. X.1b). It provides the open-circuit voltage (V_{oc}), the short-circuit current (I_{sc}), and the fill factor (*FF*); the product of these three metrics is the maximum power produced by the solar cell (Fig. X.1c). If the material properties of the solar cell are known, the thermodynamic limits for these metrics can be calculated[12, 13] to analyze the solar cell's experimental performance and diagnose areas for improvement. Efficiency (η), which is the maximum power produced by the solar cell divided by the power of the light incident on it, is the most important metric of performance. Since the two primary processes in a solar cell are generation of electron-hole pairs and their collection, measuring both the wavelength-dependent absorption of the solar cell and its efficiency at each wavelength, referred to as the external quantum efficiency (EQE) or incident photon-to-current conversion efficiency (IPCE), allows the calculation of the wavelength-dependent internal quantum efficiency (IQE) or absorbed photon-to-current conversion efficiency (APCE). While EQE provides the net performance of the solar cell that comprises effects from both absorption and charge collection, IQE indicates how well the solar cell collects charges once they are generated.

Research into nanowire PV falls into two categories: nanowire array solar cells and single-nanowire devices. Although other designs have been proposed,[14, 15] conventional nanowire array cells consist of vertical nanowires electrically contacted in parallel so that they generate currents comparable to thin-film PV cells. These devices are the most relevant for calculating efficiencies and comparing metrics with planar solar cells, and they take advantage of the improved charge collection, transport, and light trapping that occurs in nanowire films. In contrast, single-nanowire solar cells offer fundamental information about the optical and electronic properties of the solar cell's materials and the quality of its charge-separating junction. They provide insight into improving the performance of array solar cells.

X.3 Principles of Artificial Photosynthesis

Photovoltaics converts sunlight into electricity, but transforming solar energy directly into chemical fuels is also important. The direct conversion of sunlight into energy stored within chemical bonds, termed artificial photosynthesis,[16-20] mimics natural photosynthesis that occurs in plants.[21] This concept was originally demonstrated in the 1970s, using TiO_2 as a photocatalyst to split water into H_2 and O_2.[22]

The classic operation of a PEC cell used for artificial photosynthesis takes advantage of the semiconductor/electrolyte interface and resembles a photovoltaic: a photocatalytic semiconductor is immersed in an electrolyte, which forms a built-in electric field at the semiconductor/electrolyte interface (Fig. X.2a). Light absorbed by the semiconductor produces electron-hole pairs, and the built-in field at this junction separates the charges so they can perform separate chemical reactions: an oxidation and a reduction. Typically, the minority carrier reacts at the surface of the semiconductor while the majority carrier travels through the bulk of the semiconductor electrode and performs the complementary reaction at a counter electrode (Fig. X.2b). Alternatively, two light-absorbing semiconductors can be used in the biomimetic "Z-scheme": one semiconductor acts as a photocathode for reduction and the other as a photoanode for oxidation (Fig. 2c).[18, 23-26] In each of these electrodes, photoexcited minority carriers move to the solution for the half-reactions, while majority carriers recombine at the interface connecting the light absorbers. Often the surfaces of the electrodes are decorated with co-catalysts to facilitate the chemical reactions. Since the product of a PEC cell is a chemical fuel rather than electricity, the entire structure can be miniaturized into powder form. This version is particularly attractive because it is extremely low cost: powder is mixed into electrolyte and, upon exposure to sunlight, produces chemical fuels. Disadvantages include the high losses to back-reactions since the cathode and anode are in close proximity and the difficulty of separating and collecting the product fuel.

[Figure X.2 near here]

In contrast with a photovoltaic cell, the efficiency of a PEC cell can be benchmarked in different ways.[27] For an individual photoelectrode that facilitates a redox half-reaction, e.g. reducing H^+ to H_2 or oxidizing H_2O to O_2, the efficiency of the PEC device can be calculated in the same way as that of a solar cell, taking the thermodynamic electrochemical potential of the redox species as the short-circuit condition. This measured efficiency can be interpreted as the efficiency of the photon's assistance in driving the redox reaction, neglecting the additional energy required for the other half-reaction to maintain charge neutrality. In this context, this calculated efficiency is in accord with the efficiency of conventional electrochemistry, which uses a three-electrode setup. The efficiency of the sunlight-to-fuel conversion process, however, can also be defined as the overall energy stored in the chemical bonds of the produced fuel, normalized to the energy density of the incident photons. Here the efficiency is defined in the context of the overall chemical reaction rather than a redox half-reaction; this method is relevant to the full process of artificial photosynthesis.

Artificial photosynthesis shares similarities with photovoltaics, but it has additional flexibilities as well as restrictions. Both processes require absorption of light and use a junction's built-in electric field[28] to separate photogenerated charges; however, since in artificial photosynthesis a liquid electrolyte facilitates the electrochemical reactions,[19] the electric field is created by semiconductor/electrolyte interfaces[27, 28] or embedded solid junctions.[29, 30] The materials used must also be stable against photocorrosion in the electrolyte under illumination. Additionally, unlike photovoltaics, which aims simply to maximize overall power output, a minimum voltage is required to produce fuels from sunlight, which is imposed by the energetics of the desired chemical reaction. Driving reactions such as splitting water into hydrogen and oxygen or reducing carbon dioxide into organic fuels requires thermodynamic potentials greater than 1V. To overcome the kinetic barrier to achieve a high reaction rate, an electrochemical overpotential is also required.[31] This voltage restriction limits the choice of materials to semiconductors with wide band gaps if only one light-absorber is used.[32] To achieve high efficiency, however, two light-absorbers with small band gaps can provide the voltage for the chemical reaction in the "Z-scheme."[32, 33] This design means that many materials with small band gaps developed in photovoltaic research could be used, provided they are stable in the electrolyte. The additional flexibility of the "Z-scheme" design makes it a promising approach for converting solar energy into chemical fuels.

Implementing the "Z-scheme" for artificial photosynthesis is an engineering challenge that comprises the optimization and integration of many components. It requires maximizing and matching the voltage and current performance of the photocathode and photoanode, as well as pairing them with appropriate catalysts, and all of these components must be functional and stable under the same operating conditions. In nature, the photosynthetic components in chloroplasts are carefully arranged: photosystems I and II exist side by side on the thylakoid membrane with the electron transport chain between them for efficient charge transfer, while the reduction and oxidation catalytic centers are spatially separated to minimize undesirable back-reaction of the photosynthetic products.[17, 21, 30] Achieving such microscopic spatial control is a critical goal in artificial photosynthesis. Once researchers understand the behavior of nanoscale PEC systems on a modular level, they can then examine and engineer how these components interact at the system level.[34] The final achievement will be assembling all the pieces to demonstrate an optimized integrated system for artificial photosynthesis.

X.4 Nanowires for Solar Energy Conversion: Commonalities between Photovoltaics and Artificial Photosynthesis

The similarities between PV cells and PEC cells used for artificial photosynthesis mean that certain features of nanowires can be beneficial to both technologies.

X.4.1 Charge Collection and Transport

[Figure X.3 near here]

One of the key advantages of nanowires for the conversion of solar energy is their potential for more efficient separation and collection of photogenerated charges. Radial junctions orthogonalize the directions of light absorption and charge separation: absorption occurs along the long axis of the wire, while the photogenerated minority carriers travel only the radial distance to be separated and collected (Fig. X.3).[35] Once separated, the now majority carriers have a direct path to their electrode through the continuous and conductive core of the nanowire. Materials whose optical absorption length is much longer than their minority carrier diffusion length benefit most from this geometry, but it is still useful for materials with excellent absorption and transport such as GaAs.[36] Because the core-shell geometry relaxes the requirements on minority carrier diffusion length,[35] nanowires can allow solar cells or photoelectrodes to be made from materials that are unsuitable in a planar geometry. In PV, candidates include sulfides,[37] oxides,[38] and low-purity[39] or heavily doped silicon,[40] which have the advantages of being inexpensive and abundant in the earth's crust. Dye-sensitized solar cells[41-43] and semiconductor-organic hybrid solar cells[44] also employ this geometry in order to improve charge collection from the dye or low-mobility organic phase. Such an idea of sensitizing a conductive nanowire scaffold has also been used in photoelectrodes, in which the surrounding electrolyte forms a core-shell-shell structure.[45, 46]

[Figure X.4 near here]

Equivalent circuit models are used to describe the transport of electrons within a PV or PEC cell and to analyze how to improve its performance (Fig. X.4a). In a solar cell, the *p-n* junction is a rectifying diode because the built-in electric field allows current to flow appreciably in only one direction. The forward bias current increases exponentially as the applied bias counteracts the built-in potential of the junction, lowering the barrier for carriers to diffuse across it (diffusion current).[10] The reverse saturation current arises from thermally generated carriers that drift to their respective contacts via the built-in field (drift current). Additional diodes, which can also be conceptualized as voltage-dependent variable resistors, can be added in parallel with the drift-diffusion diode to represent recombination processes, such as the recombination within the depletion region[10, 47] or at grain boundaries.[48] Shining light on the solar cell generates a constant flow of electrons and holes, modeled as a current source that opposes the diode's diffusion current and shifts the *I-V* curve on the current axis.

Resistance that impedes transport through the quasi-neutral regions of the solar cell or its contacts is labeled series resistance and reduces the current output and fill factor of the solar cell. Stray current paths that bypass the potential of the junction lower the solar cell's shunt resistance and reduce its open-circuit voltage and fill factor. The ideal diode model of a solar cell exhibits no series resistance and infinite shunt resistance; for best performance from a practical standpoint, the series resistance should be much smaller and the shunt resistance much larger than the characteristic resistance of the solar cell (R_{ch}), which is given by V_{oc}/I_{sc}.[49, 50] In the equivalent circuit of a photoelectrode, the semiconductor/electrolyte junction functions as a diode, the electrochemical charge transfer behaves as a voltage-dependent series resistor, and the recombination of photogenerated carriers acts as a voltage-dependent shunt resistor. An additional series resistance from mass transport limitations can also arise under conditions of intense illumination or low concentration of redox species.[51] The high surface area of an array of nanowires can reduce series resistance and therefore increase the photocurrent curve's fill factor by allowing more chemicals to be produced at a lower voltage. Both this reduced overpotential and more efficient charge collection are reasons cited in the literature for the enhanced performance of nanostructured electrodes as compared to planar benchmarks (Fig. X.4b-d).[27, 52]

Radial junctions offer many opportunities for improved PV and PEC cells, but careful design and control over material properties are necessary to realize their benefits. To avoid degrading the device's efficiency with low built-in voltage or high series resistance, fully depleting the carriers of either side of the junction must be avoided. Because of their small size, the core or shell of a nanowire with low carrier concentration can be easily depleted if the junction's other side is more heavily doped. For this reason, the core and shell thicknesses and doping levels or redox concentrations must be carefully controlled to ensure optimized performance.[12,19]

Additionally, interface and surface states play a much larger role in nanowire devices than in their planar counterparts. Nanowire PV and PEC cells are particularly sensitive to depletion-region recombination because of their large junction area.[35, 53] In PV, experimental work on silicon and CdS/Cu_2S single-nanowire solar cells indicates that the quality of the junction is crucial to their efficiency. By controlling the crystallinity of the shell and the abrupt doping structure of the homojunction, the V_{oc} of *p-i-n* silicon single-nanowire solar cells has improved from 260 mV to up to 500 mV and the *FF* from 55% to 73%.[54,55] These figures still trail those of planar crystalline silicon PV, whose record values are 706 mV and 83%,[56] and such a difference is typical for single-nanowire solar cells produced from other materials such as GaAs[57, 58] and the $GaN/In_xGa_{1-x}N$ system.[59] $CdS\text{-}Cu_2S$ single-nanowire solar cells, however, exhibit V_{oc} and *FF* values that slightly exceed those of their planar counterparts, which is attributed to their high-quality heteroepitaxial junction.[37] In PEC, this principle translates into control of the semiconductor-electrolyte interface, and it has been demonstrated that without consideration of the interface, a nanowire electrode may not outperform a planar one.[60, 61] Electrochemical impedance spectroscopy can be used to understand the role of surface states,[61-63] and the interface should be engineered to minimize detrimental effects such as surface recombination[64] and Fermi-level pinning.[65] Work on TiO_2 photoanodes has demonstrated improved performance by modifying the surface with TiO_2 deposited by atomic layer deposition (ALD),[66] and applying catalysts to the electrode's surface is also a form of engineering the interface to reduce surface recombination. Another common strategy for junction engineering adds a core-shell heterojunction at the semiconductor/electrolyte interface to produce an additional built-in field for charge separation.[67, 68] Sometimes the shell is also designed as a sensitizer, allowing light to be absorbed at the surface, while the conductive core provides charge transport along the wire's length.

One challenge inherent to charge collection within a nanowire array is its dilution of photogenerated carriers across a larger interface, resulting in lower V_{oc} or photovoltage as compared to planar PV or PEC cells.[55] Assuming that the dominant recombination mechanisms in the planar and nanowire solar cells are the same, which is an assumption that depends on the specific material system,[60] this effect is analogous to a planar cell with the equivalent junction area operating in lower light conditions. Because of the chemical reaction that occurs in PEC cells, this disadvantage is counterbalanced by the lower overpotential required to perform that reaction. No such mitigating factor exists for PV, however, suggesting that concentration of incident light might improve the efficiency of nanowire solar cells.

X.4.2 Light Trapping in Nanowire Arrays

Nanowires in ordered or random arrays exhibit light-trapping effects because of their microscopic arrangement and sub-wavelength diameters. These effects allow a film of nanowires to absorb more light than would a thin film made from the equivalent volume of material. A portion of this increase arises from the nanowires' acting as an anti-reflection coating, which can be understood as grading the refractive index difference between air or the electrolyte and the material of the nanowire;[69, 70] however, the specific geometry of the interfaces within the nanowire film dictates the film's optical modes, which also lead to increased absorption.[71] The record nanowire solar cell, made from InP nanowires with axial *p*-*i*-*n* junctions (Fig. X.5), relies on light trapping: its nanowires cover only 12% of the area of the cell but produce 83% of the short-circuit current of the best InP planar cells.[72] Although even random arrays exhibit light trapping, carefully engineered arrays in theory can exceed the light trapping of a randomly textured surface[73] and produce a nanowire solar cell whose efficiency exceeds that of its planar counterpart.[74, 75] Much experimental work has demonstrated increased absorption within nanowire and microwire films.[72, 76-78]

[Figure X.5 near here]

X.4.3 Approaches for Reducing Costs

The commercial relevance of a solar technology depends both on its efficiency and its cost of implementation.[3] Even the most efficient technologies, such as multijunction concentrator solar cells, are not in widespread use because they are still prohibitively expensive.[79] Lower production costs, as compared to crystalline silicon modules, have driven the expansion of the thin-film PV industry,[80, 81] and nanowires can be viewed as the natural heir in this succession of inexpensive, yet efficient technologies. PEC cells that convert sunlight directly into chemical fuels, rather than using an electrolyzer coupled to a PV cell, and in particular powder photocatalysts, are a way to reduce the complexity and cost of solar energy conversion even further. The extensive literature on low-temperature, solution-based, and scalable syntheses of nanowires indicates that nanowire PV and PEC cells will ultimately be less expensive to produce than their thin-film counterparts. In addition, the unique optical and transport properties of nanowires will allow less actual material to be used in a PV or PEC cell to achieve similar efficiencies.[72, 74] The development of scalable atomic layer deposition (ALD) processing also bodes well for nanowire PV and PEC cells because it can coat high-aspect-ratio nanowire arrays with ultrathin semiconductor films to form transparent contacts, heterojunctions, or encapsulation layers.[82, 83] It also provides a method for loading catalytic materials uniformly along high-aspect-ratio structures and offers unprecedented control over small loading amounts of expensive catalysts such as Pt.[84] Finally, like organic solar cells and some thin-film PV, nanowire array cells can be produced using lightweight, flexible substrates that will make them less expensive to implement and suitable for mobile applications.[85]

X.5 Single-Nanowire Photovoltaics

Single-nanowire devices are useful platforms with which to study the electrical and some of the optical properties of nanowire PV cells. The typical device geometry in which the nanowire lies flat on an insulating substrate does not capture the benefits of orthogonal light absorption and charge separation, but it does provide a way to investigate the quality of the charge-separating junction, the charge transport through the nanowire, and the wavelength-dependent photocurrent of the nanowire solar cell. Since the fabrication of array solar cells can be plagued with difficulties in reducing series resistance and maximizing shunt resistance, single-nanowire solar cells allow some fundamentals of the material system to be investigated before extensive effort is put into developing an array solar cell.

X.5.1 Transport within Single-Nanowire Solar Cells

Current-voltage (*I-V)* curves of single-nanowire solar cells determine if the chosen material junction rectifies and separates photogenerated carriers. Reducing parallel and series resistances in single-nanowire solar cells is simpler than in an array device. While low shunt resistance often obscures rectifying behavior in array solar cells, the shunt resistance of single-nanowire solar cells arises from the quality of the material junction since much spatial separation exists between the top and bottom contacts. Series resistances are also less important than in array solar cells because single-nanowire devices source only pico- or nanoamperes of current; consequently, their junction's characteristic resistance is many orders of magnitude larger than that of an array solar cell, allowing the I_{sc} and FF to remain relatively unaffected by kilo- or even mega-ohm series resistances. Additionally, ohmic behavior and quantitative contact resistance at the metal/semiconductor interfaces can be evaluated by four-point resistance measurements on the devices. Although absorption of light in single-nanowire solar cells can be a challenge because of the small path length and potentially small active area for axial junctions, power and temperature dependencies of the solar cell's parameters under concentrated light sources can still offer insight into the junction quality. Because the excitation geometry of typical single-nanowire solar cells does not match that of an array device, efficiency estimates based on single-nanowire solar cells are less relevant. Also, since single-nanowire solar cells are typically smaller in diameter than the wavelength of light in the visible spectrum, their absorption cross-section can exceed their geometrical cross-sectional area, which increases their apparent efficiency.[55]

X.5.2 Optical Properties of Single Nanowires

[Figure X.6 near here]

Because of their subwavelength dimensions, single nanowires exhibit optical resonances in the visible portion of the spectrum that increase their absorption of light. These resonances are modeled as the electromagnetic modes of a dielectric cylinder and can be either bound modes or leaky modes, depending on whether their propagation constant is real or complex, respectively.[86] Bound modes confine and guide incident light along the axis of the cylinder, while leaky modes allow energy to radiate from the system as the light propagates along the wire.[14, 58, 87-89] At the wavelengths of these resonances, the nanowire's absorption cross-section is much larger than its geometrical cross-section, essentially concentrating light within the wire. The positions and intensities of these modes depend sensitively on the nanowire's refractive index and diameter,[14, 55, 90] but similar trends are seen for nanowires with various cross-sectional geometries (Fig. X.6).[14] Two- and three-dimensional numerical electromagnetic simulations, which solve Maxwell's equations for the light-wire system, can be used to predict enhancements in absorption that agree well with experimental results.[55, 88] These resonances increase the estimated efficiency of a single-nanowire solar cell because they allow the wire to collect light from beyond its geometrical cross-section, meaning that the external quantum efficiency of the wire can exceed unity at resonance wavelengths even when the internal quantum efficiency is lower and limited to unity (Fig. X.6d).[55, 58] This increase in single-wire efficiency, however, does not necessarily translate into more efficient array solar cells. Using these modes to improve the efficiency in array devices implies sparse coverage of a substrate with nanowires, since dense arrays would make the concentrating effect unnecessary. In this case, since nanowire solar cells operate more efficiently under concentrated light, an array device might perform better by concentrating light into a few nanowires rather than harvesting dilute light over a dense array of many nanowires.[58, 75] Achieving such an optimal architecture requires predicting the diameter and pitch of the nanowire array necessary to create sufficient concentration of light within the nanowires, as well as experimental realization of such a design. Numerical electromagnetic simulations will therefore continue to play a key role in the design of nanowire PV, although they must be complemented with synthetic techniques that can achieve spatial control over the growth of regular nanowires. The next step will be to integrate electromagnetic simulations with models of the device physics to understand where charges are generated within the wires so that they can be collected most effectively.[91]

X.6 Nanowires for "Z-scheme" Artificial Photosynthesis: Electrochemical Considerations

X.6.1 Stability Against Photocorrosion

In contrast to PV cells that can be encapsulated to protect them from degradation by the elements, PEC photoelectrodes must remain stable during operation in an electrolyte under illumination. The oxidative environment at the photoanode is particularly corrosive and suggests the use of a stable protection layer, especially for compound semiconductors in aqueous electrolytes. The technique of atomic layer deposition (ALD),[92] with its capability to form uniform, pinhole-free coatings on high-aspect-ratio nanostructures, is a particularly promising approach for protection layers, as demonstrated in the case of a Si photoanode[83] and a Cu_2O photocathode.[93]

X.6.2 Principles of System Design

To optimize the performance of the "Z-scheme" in artificial photosynthesis, charges should move through the multi-component system unhindered. Achievement of this goal requires matching the charge flux between the current-generating light-absorbers and the current-consuming electrocatalysts. At the same time, current densities between the two light absorbers must also be matched while they maintain a voltage sufficient to perform the desired chemical reaction. Nanowires offer several new possibilities for tackling these challenges.

Generation of photoexcited carriers within a semiconductor is typically much more rapid than the chemical reaction that occurs at the electrocatalyst on the photoelectrode's surface. A solar-to-fuel efficiency of 5-10%, which is considered the lower limit for a commercially viable PEC technology,[6, 94, 95] corresponds to a photogenerated flux of ~10 mA/cm^2 under 1-sun illumination, equivalent to 620 electrons nm^{-2} sec^{-1}. The typical density of surface atoms on a material is ~10^{15} atoms cm^{-2}, or equivalently 10 atoms nm^{-2}. This sets a ~62 sec^{-1} lower limit for the electrocatalyst's turn-over frequency (TOF) on a planar electrode, assuming that all surface atoms are electrochemically active. Practically, a higher TOF is needed because many surface atoms are inactive, a reduced co-catalyst loading might be necessary to avoid blocking the photon flux, or to reduce the cost from an expensive co-catalyst. To achieve a higher TOF and therefore a higher current density, an increased overpotential is required based on the Butler-Volmer equation,[31] which reduces the system's energy conversion efficiency. Based on the data of several electrocatalysts used for hydrogen evolution,[96-101] oxygen evolution,[102-108] and CO_2 reduction,[109-111] a non-negligible overopotential loss may be present because of an inadequate TOF (Fig. X.7). A nanowire array electrode reduces the overpotential required for a given rate of solar-to-fuel conversion[34] because the same light-induced current density passes through the larger surface area of a nanowire electrode, reducing the TOF demanded of the electrocatalyst. Nanowire electrodes therefore facilitate reactions that are kinetically slow,[112] reducing the required loading amount of noble-metal electrocatalysts[84] or allowing the substitution of less active earth-abundant materials.[113, 114] Creating branched nanowire structures increases the surface area further, which improves the electrode's saturation photocurrent and fill factor[112] because of enhanced charge collection and reduced series resistance from the electrochemical reaction. Demonstrations of the benefits of high-aspect-ratio nanostructures have been reported in many material systems, including TiO_2,[112] hematite (n-Fe_2O_3),[115, 116] ZnO,[117, 118] WO_3,[119, 120] GaAs,[36] GaP,[121, 122] GaN,[123, 124] and Si,[62, 125-130] confirming the generality of this approach.

[Figure X.7 near here]

Optimized use of the "Z-scheme" also requires matching the flux between the photoanode and photocathode. The two materials must possess suitable band gaps and a low-resistance pathway for their majority carriers to recombine.[131] Theoretical calculations that account for overpotentials and other losses,[33, 94] propose target band gaps for a pair of electrodes of around 1.1 eV and 1.7 eV, but the selection of appropriate binary materials with band gaps ranging between 1.5 eV to 2.0 eV is limited (Fig. X.8). In addition, driving the chemical reactions in artificial photosynthesis requires a minimum voltage, so both the band gaps of the materials and their band alignment and resultant photovoltage are important.

[Figure X.8 near here]

While photocathodes are well developed, the improvement of photoanodes deserves more attention.[132] Photocathodes of Si[127, 133] (E_g = 1.1eV) and InP[134] (E_g = 1.3eV) generate high current densities with photovoltages exceeding 500 mV. Research on photocathodes therefore focuses on reducing the use of raw materials and fabrication costs, for example through the low-cost solution-phase synthesis of semiconductor nanomaterials.[121, 122] In contrast, currently no stable photoanode can produce a photocurrent greater than 10 mA/cm^2, while also providing adequate photovoltage to couple with a photocathode. Oxide and nitride materials are the conventional photoanodes because of their stability against photocorrosion and appropriate valence band positions, yet their large band gaps limit the maximum photocurrent they can produce and their intrinsically low hole mobility, arising from the localized *p*-orbital nature of their valence band, impedes charge transport.[135] Novel materials, such as ternary semiconductors with tunable band gaps or corrosion protection layers for unstable existing semiconductors, are key areas of development in photoanode research.

X.7 Progress in Nanowire Photovoltaics and Artificial Photosynthesis

In the Yang Laboratory early work on dye-sensitized solar cells (DSSCs) was the beginning of a path toward PV and PEC cells using nanowires.[9, 136] A DSSC represents something of a hybrid technology between a solid-state PV cell and a PEC cell. Although it outputs electricity like a conventional solar cell, a DSSC relies on a redox reaction at the surface of a semiconductor, similar to a PEC cell. In a conventional DSSC, light absorbed by an organic dye excites an electron in the dye. This excited electron is then injected into a nearby metal-oxide film and collected by the underlying electrode. A redox couple in solution, often I^-/I^{3-}, reduces the oxidized dye to close the circuit. In this way, light absorbed by the dye generates a current and voltage in the DSSC. The interfacial structure of the sensitized electrode and the electronic structure and light absorption of the dye determine the efficiency of the DSSC.[137] Electrodes made of metal-oxide particulates are typically used because their extensive surface area allows adsorption of large quantities of dye, which increases the light absorption of the DSSC. In order for the photoexcited electron from the dye to be collected, however, the electron must be transferred to the metal oxide and pass through the electrolyte-bathed metal-oxide electrode to the underlying contact without recombining; consequently, the distance from the dye to the back contact must be less than the characteristic carrier diffusion length within the nanoparticulate film, which is typically ~10 μm.[138] Sensitizing such a thin film with enough dye to absorb all the light in the solar spectrum, particularly in the red and infrared regions, however, remains a challenge. Thus DSSCs exhibit a mismatch between the length scales required for absorption of light and collection of charges. A DSSC fabricated using ZnO nanowires as the electron-collecting electrode exhibited better charge collection than ZnO nanoparticulate films, pioneering the use of nanowire arrays to achieve collection of charges through an optically thick absorption layer (Fig. X.9).[136] Additionally, faster electron injection from the dye into the ZnO nanowires than into ZnO nanoparticle films reinforced the critical role that surfaces play in electrochemical reactions. These observations of the benefits of geometry and sensitivity to interfacial structure proved foundational for subsequent work on nanowire PV and PEC cells.

[Figure X.9 near here]

After the promising results of improved charge transport in the ZnO nanowire DSSC, the next step was to understand the role that interfaces play in solar energy conversion devices. A detailed study of DSSCs produced from ZnO nanowire arrays overcoated with either Al_2O_3 or TiO_2 demonstrated that such interfacial layers strongly affect the device's efficiency.[9] Al_2O_3 acts as a blocking layer both for recombination as well as charge transfer, yielding increased V_{oc} but lower J_{sc} and efficiency. Layers of anatase TiO_2 with optimized thickness, however, increased the efficiency by yielding higher V_{oc} and comparable J_{sc}. The TiO_2's crystallinity was essential to achieving good electronic injection and transport, and the n^+-n junction between the ZnO and TiO_2 provided a built-in electric field to drive electrons away from the surface, reducing their rate of recombination. A similar result was obtained in the study of photoanodes for water oxidation fabricated from Si nanowires coated in TiO_2.[45] The n-Si/TiO_2 heterojunction produces a built-in field that helps channel majority carriers away from the surface to minimize recombination with the minority carriers that perform the PEC reaction. The built-in potential of the illuminated n-n^+ junction also provides a boost to the V_{oc}. Reinforcing the optical advantages of nanowires, the nanostructured electrodes' high surface area and therefore larger area of TiO_2, as well as their low reflectance, produced increased photocurrent in comparison to planar control samples.

Investigations into nanostructured solid-state solar cells have also suggested the critical importance of interfaces. ZnO-P3HT (Poly(3-hexylthiophene)) nanorod array solar cells were rectifying only with the addition of a TiO_2 interlayer to improve the charge separation at the inorganic-polymer interface.[139] Careful engineering of the ZnO-P3HT interface by chemical grafting produced rectifying devices with higher V_{oc} and FF than array devices.[44] This improvement can be attributed either to the fewer available shunt paths in these devices as compared to array solar cells or to the higher quality of the grafted interface; however, array solar cells whose ZnO nanowires were coated with ALD ZnO to reduce shunt resistance paths through the substrate performed similarly poorly,[139] and work by other groups has confirmed the sensitivity of charge separation and device performance to modification of the ZnO-P3HT interface.[140, 141] Similar results were found in the case of solar cells made from ZnO nanowires and Cu_2O nanocrystals. Without an intervening layer of crystalline TiO_2 deposited by ALD, the solar cells exhibited almost negligible photocurrent and photovoltage, but the efficiency increased over fifty times upon the addition of 10 nm of TiO_2.[142] While this improvement can be attributed to an increase in the shunt resistance of the array solar cell, it is possible that the mechanism of this increase in resistance is similar to that found in the n-Si/TiO_2 photoanodes: the n-n^+ junction siphons electrons away from the interface, making them less likely to recombine at the Cu_2O/ZnO junction and increasing the shunt resistance. Lastly, single-nanowire CdS/Cu_2S solar cells have also confirmed the importance of junction quality in producing devices with high efficiency.[37] CdS nanowires were exposed to CuCl solution in a low-temperature, aqueous cation-exchange reaction in which the Cu^+ cations replace the Cd^{2+} cations while the sulfur sublattice remains intact. In single-crystalline CdS nanowires, this reaction produces an epitaxial heterojunction in which both sides are single crystals with few defects at the interface. The structural quality of the heterojunction produced V_{oc} and FF values that surpassed the literature values for planar solar cells produced using this method, demonstrating the benefit of nanoscale interfacial control (Fig. X.10). Although the single-nanowire solar cell's efficiency suffered from poor light absorption as a result of its thin Cu_2S shell, integrating such structures into an array solar cell to increase absorption would likely remedy this deficiency.

[Figure X.10 near here]

Dramatic improvement was also found between first- and second-generation silicon nanowire array solar cells. Initially, silicon nanowires were produced using electroless etching, which leaves extremely rough surfaces.[143] The *p*-*n* junction was then created by depositing a *p*-type polycrystalline film onto the *n*-type wires, yielding 0.5%-efficient solar cells with 0.29 V V_{oc}, 4.28 mA/cm^2 J_{sc}, and 0.33 FF.[144] When nanowires were etched from wafers using the Bosch process (Fig. X.11a,b), which yields much smoother surfaces, and the junction made through high-temperature diffusion rather than deposition of a polycrystalline film, efficiencies reached 5% with V_{oc} 0.52 V, J_{sc} 16.82 mA/cm^2 and FF 0.61.[77] Some of the J_{sc} and FF increase can be attributed to reduced series resistance in the *p*-type shell and the *n*-type core of the nanowires, while about ~150 mV of the V_{oc} can be attributed to the shorter and thicker wires used in the second-generation solar cells. Wires with less surface area offer less junction area for recombination, which directly influences the dark current of the solar cell and therefore its V_{oc}. It is also possible that the single-crystal quality of the diffused junction contributed to its better performance, in comparison with the polycrystalline junction in the original array solar cells, which is consistent with single-wire measurements on silicon nanowire solar cells.[55]

[Figure X.11 near here]

The better performance of the silicon nanowire array solar cells then allowed their light trapping properties to be studied in detail. Longer nanowires clearly showed less transmission in the red region of the spectrum, but a tradeoff existed between increased photocurrent from light absorption and decreased V_{oc} and FF from junction and surface recombination (Fig. X.11c,d). By varying the thickness of the nanowire films, the enhanced path length could be calculated; for nanowires with roughness factors ~30 it was found to exceed the limit of purely randomized light trapping. This work demonstrated experimentally and quantitatively the significant enhancement in photocurrent that can be produced by nanowire arrays, which is important for increasing efficiency in both PV and PEC cells.

Nanowires themselves exhibit light trapping because of their size and periodicity in arrays, but even more strongly absorbing systems can be constructed by coupling nanowires with nanoscale metal particles and thin films. Metal nanostructures support collective excitations of the free electrons at their surface, known as surface plasmons. Light's alternating electromagnetic field can drive this collective electronic motion and transfer its energy to the surface plasmons, whose resonance frequencies depend on the metal's free electron density and band structure, the nanostructure's size and shape, and the local dielectric environment.[145-149] By changing these characteristics, the resonances of metal nanostructures are tunable throughout the visible and near-infrared regions of the spectrum. Excitation of surface plasmons creates intense evanescent fields near the nanostructure's surface as well as increased scattering and absorption cross sections.[150] Both evanescent and scattered fields have been shown to enhance absorption of light within the surrounding dielectric media,[151-153] meaning that plasmonic structures function like frequency-dependent nanoscale light concentrators. This concentration leads to higher energy conversion efficiencies in PV and PEC cells, which can be demonstrated by measuring the photocurrent as a function of wavelength. For example, thin films of iron oxide (Fe_2O_3) were coated onto gold nanorods to improve the films' absorption of light and performance as a photoanode.[154] Fe_2O_3 is known for its small minority carrier diffusion length,[155] so the larger surface area of the nanorod geometry offered better charge collection, while the plasmonic resonance of the gold nanorods increased the absorption of light near the band gap of Fe_2O_3 (Fig. X.12a,b).[154] When coupling plasmonic nanostructures with absorbing materials that exhibit their own optical resonances, however, the combined system must be designed carefully in order to avoid decreasing absorption in the active material. Decorating a silicon single-nanowire solar cell with an octahedral silver nanocrystal decreased absorption at the nanowire's own optical resonances, while it increased absorption at the resonances of the nanocrystal (Fig. X.12c,d).[90] This fundamental study highlighted the importance of performing detailed simulations of any proposed dielectric-metal nanostructure in order to ensure that the system will increase absorption rather than reduce it. To achieve the most complete understanding of solar cells with nanoscale dimensions, the next step is to integrate electromagnetic simulations with simulations of the device physics to optimize where charges are generated and collected within the solar cell. As such calculations become more routine, they will offer a powerful way to screen new designs.

[Figure X.12 near here]

Nanowires also provide benefits in the development of new materials for PV and PEC applications and low-cost methods for producing old ones. Gas-phase[36, 156] or liquid-phase[121] syntheses can yield single-crystalline nanowires of high electronic and optical quality. III-V semiconductor alloys, such as $In_xGa_{1-x}P$ and $In_xGa_{1-x}N$,[157] with tunable band gaps between 1.5 and 2.0 eV, are of particular interest for artificial photosynthesis, in addition to compound III-V semiconductors such as GaAs[36] and GaP.[121, 122] A liquid-phase synthesis of large quantities of surfactant-free GaP nanowires was demonstrated,[121] which also allowed careful control of carrier type and concentration through the addition of dopant precursors during the synthesis (Fig. X.13).[122] Such doping control is crucial for any core-shell heterostructure, both in PEC and PV, to ensure that the core remains conductive for charge collection. This synthesis, which can be extended to other compound semiconductors, offered a new approach to produce low-cost III-V materials for solar energy applications.

[Figure X.13 near here]

With the synthetic development of nanowire versions of well-understood materials such as silicon and TiO_2, the precise influence of the nanowire geometry on PEC performance could be more fully investigated. Current matching between the photogenerated flux of the electrode and the TOF of the catalyst is one way that nanowires can offer improved efficiency. With this concept in mind, the loading of Pt nanoclusters onto Si nanowire photocathodes for hydrogen evolution was investigated quantitatively.[84] A conformal coating of Pt nanoparticles with sizes ranging from 0.5-3 nm was deposited using atomic layer deposition (ALD) (Fig. X.14a). The electrochemical and photoelectrochemical performance were measured using as little as 1 cycle of ALD Pt, which corresponds to a surface mass loading of ~10 ng/cm^2, or equivalently about 2.7% of a monolayer of surface coverage (Fig. X.14b). Despite these low Pt loading quantities, Si nanowire photocathodes still yielded sufficient photocurrent for solar-to-fuel conversion, and varying the sub-monolayer Pt mass loading controlled the slope of the *J*-*V* curve. This exploration of the lower limits of Pt co-catalyst loading on high-surface area nanowire photoelectrodes established a general approach to minimize the cost of precious metal co-catalysts.

[Figure X.14 near here]

After much work studying and improving the individual components necessary for artificial photosynthesis, the culminating step was to produce a prototype integrated system. Work toward this goal began with the fundamental study of an asymmetric nanowire composed of a silicon core coated with a TiO_2 shell (Fig. X.15a-c). This structure is a minimized photocathode (*p*-Si) and photoanode (*n*-TiO_2) linked together at a nanoscale interface. Kelvin probe force microscopy verified the "Z-scheme" motion of charges when the asymmetric structure was illuminated: minority holes moved to the surface of the TiO_2, increasing its surface potential, while the majority electrons recombined at the Si/TiO_2 interface. Building on this fundamental study, similar Si and TiO_2 heterostructures were used to demonstrate solar water splitting in an integrated nanosystem (Fig. X.15d-f).[26] Fundamental knowledge of the system's interfaces[45, 131] was applied to fabricate tree-shaped nanowire-based heterostructures that were loaded selectively with electrocatalysts for hydrogen and oxygen evolution. Established design principles of nanowire photoelectrodes[60] motivated the use of small TiO_2 nanowires: TiO_2 possesses a shorter minority carrier diffusion length than Si, and the oxygen evolution reaction exhibits slower reaction kinetics than hydrogen reduction. The ultraviolet band gap of the TiO_2 photoanode also limited the overall current density and solar-to-fuel conversion efficiency, which was 0.12% and comparable to that of natural photosynthesis.[17, 21] The key advantage of this this proof-of-concept integrated device is that improvement can be achieved by updating individual components, such as replacing the TiO_2 nanowires with an improved nanostructured photoanode.[34]

[Figure X.15 near here]

In the past eight years, much fundamental insight has been gained into the basic components of nanowire PV and PEC cells. Now the task ahead is to implement these lessons in increasingly complex and integrated designs. Aided by the development of numerical simulation tools and the rapid increase in available computing power, researchers can now predict the best nanowire length or doping level for a specific application. Yet significant challenges remain: the optoelectronic properties of unconventional semiconductors, the chemistry of interfaces, and the system-level[34] interactions within integrated structures are all areas awaiting further exploration and insight.

X.8 Future Outlook

With the world's need for renewable energy becoming ever more urgent, the time is fast approaching to realize the full potential of nanowire photovoltaics and artificial photosynthesis. Success begins with the right materials, including newly synthesized light-absorbers and catalysts. For widespread application, these materials will need to be made from relatively abundant elements and processed inexpensively at large scale. Solution-processed nanowires offer a solution, but currently many of the best-performing solar devices rely on high-temperature vapor-phase techniques. Little work has been done to compare the electrical and optical properties of solution-grown nanostructures with their vapor-phase counterparts. Creating, understanding, and controlling high-quality interfaces at the nanoscale are also crucial tasks for improving PV and PEC cells. Additionally, this synthetic control must be combined with integrated device physics and optical simulations to optimize performance. Although the basic principles have been determined, simplified models will continue to fall short of predicting the nuances of real devices without a detailed understanding of interfacial charge-transfer processes. Further into the future, commercial considerations such as device stability and lifetimes, availability of materials, and production costs will need to be evaluated as well. It will take the combined, collaborative efforts of chemists, physicists, and engineers, both experimentalists and theorists, to achieve the next level of understanding in these systems and to realize the potential of nanowires for solar energy conversion.

Acknowledgements

References

1. *Annual Energy Review 2011*, U.S. Energy Information Administration, Washington, DC, 2012.
2. S. Chu and A. Majumdar, *Nature*, 2012, **488**, 294-303.
3. N. S. Lewis, *Science*, 2007, **315**, 798-801.
4. S. Price and R. Margolis, *2008 Solar Techologies Market Report*, U.S. Department of Energy, 2010.
5. R. G. Little, R. W. Collins, T. Anderson, B. Buller, G. Dennler, M. Gloeckler, N. H. Karam, S. Kurtz, D. C. Olson, T. Surek and J. Wohlgemuth, *Foundations for Innovation: Photovoltaic Technologies for the 21st Century*, National Institute of Standards and Technology, 2010.
6. R. E. Blankenship, D. M. Tiede, J. Barber, G. W. Brudvig, G. Fleming, M. Ghirardi, M. R. Gunner, W. Junge, D. M. Kramer, A. Melis, T. A. Moore, C. C. Moser, D. G. Nocera, A. J. Nozik, D. R. Ort, W. W. Parson, R. C. Prince and R. T. Sayre, *Science*, 2011, **332**, 805-809.
7. *Basic Research Needs for Solar Energy Utilization*, U.S. Department of Energy Office of Basic Energy Sciences, 2005.
8. K. Peng, Y. Wu, H. Fang, X. Zhong, Y. Xu and J. Zhu, *Angew. Chem.*, 2005, **44**, 2737-2742.
9. M. Law, L. E. Greene, A. Radenovic, T. Kuykendall, J. Liphardt and P. Yang, *J. Phys. Chem. B*, 2006, **110**, 22652-22663.
10. G. W. Neudeck, *The PN Junction Diode*, Addison-Wesley, Reading, Massachussetts, 1983.
11. M. A. Green, *Solar Cells: Operating Principles, Technology, and System Applications*, Prentice-Hall, Englewood Cliffs, NJ, 1982.
12. W. Shockley and H. J. Queisser, *J. Appl. Phys.*, 1960, **32**, 510-519.
13. A. Polman and H. A. Atwater, *Nature Mater.*, 2012, **11**, 174-177.
14. L. Cao, P. Fan, A. P. Vasudev, J. S. White, Z. Yu, W. Cai, J. A. Schuller, S. Fan and M. L. Brongersma, *Nano Lett.*, 2010, **10**, 439-445.
15. X. Zhang, C. W. Pinion, J. D. Christesen, C. J. Flynn, T. A. Celano and J. F. Cahoon, *The Journal of Physical Chemistry Letters*, 2013, **4**, 2002-2009.
16. N. S. Lewis and D. G. Nocera, *Proceedings of the National Academy of Sciences*, 2006, **103**, 15729-15735.
17. J. Barber, *Chemical Society Reviews*, 2009, **38**, 185.
18. H. B. Gray, *Nat Chem*, 2009, **1**, 7-7.
19. J. Turner, *Nat Mater*, 2008, **7**, 770-771.
20. Y. Tachibana, L. Vayssieres and J. R. Durrant, *Nat Photon*, 2012, **6**, 511-518.
21. D. Hall and K. Rao, *Photosynthesis*, 6 edn., Cambridge University Press, Cambridage, United Kingdom, 1999.
22. A. Fujishima and K. Honda, *Nature*, 1972, **238**, 37-38.
23. A. J. Nozik, *Applied Physics Letters*, 1976, **29**, 150-153.
24. A. Kudo, *MRS Bulletin*, 2011, **36**, 32-38.
25. K. Maeda, *ACS Catalysis*, 2013, 1486-1503.
26. C. Liu, J. Tang, H. M. Chen, B. Liu and P. Yang, *Nano Letters*, 2013.

27. M. G. Walter, E. L. Warren, J. R. McKone, S. W. Boettcher, Q. Mi, E. A. Santori and N. S. Lewis, *Chemical Reviews*, 2010, **110**, 6446-6473.
28. M. Gratzel, *Nature*, 2001, **414**, 338-344.
29. S. Y. Reece, J. A. Hamel, K. Sung, T. D. Jarvi, A. J. Esswein, J. J. H. Pijpers and D. G. Nocera, *Science*, 2011, **334**, 645-648.
30. D. G. Nocera, *Accounts of Chemical Research*, 2012, **45**, 767-776.
31. A. J. Bard and L. R. Faulkner, *Electrochemical Methods: Fundamentals and Applications*, 2nd edn., John Wiley & Sons, Inc., 2001.
32. J. R. Bolton, S. J. Strickler and J. S. Connolly, *Nature*, 1985, **316**, 495-500.
33. S. Hu, C. Xiang, S. Haussener, A. D. Berger and N. S. Lewis, *Energy & Environmental Science*, 2013.
34. P. Yang and J.-M. Tarascon, *Nature Materials*, 2012, **11**, 560-563.
35. B. M. Kayes, H. A. Atwater and N. S. Lewis, *J. Appl. Phys.*, 2005, **97**, 114302.
36. S. Hu, C.-Y. Chi, K. T. Fountaine, M. Yao, H. A. Atwater, P. D. Dapkus, N. S. Lewis and C. Zhou, *Energy & Environmental Science*, 2013.
37. J. Tang, Z. Huo, S. Brittman, H. Gao and P. Yang, *Nature Nanotech.*, 2011, **6**, 568-572.
38. K. P. Musselman, A. Marin, L. Schmidt-Mende and J. L. MacManus-Driscoll, *Adv. Funct. Mater.*, 2012, **22**, 2202-2208.
39. A. Boukai, P. Haney, A. Katzenmeyer, G. M. Gallatin, A. A. Talin and P. Yang, *Chem. Phys. Lett.*, 2011, **501**, 153-158.
40. H. P. Yoon, Y. A. Yuwen, C. E. Kendrick, G. D. Barber, N. J. Podraza, J. M. Redwing, T. E. Mallouk, C. R. Wronski and T. S. Mayer, *Appl. Phys. Lett.*, 2010, **96**, 213503.
41. M. Law, L. E. Greene, J. C. Johnson, R. Saykally and P. Yang, *Nat Mater*, 2005, **4**, 455-459.
42. C. H. Peters, A. R. Guichard, A. C. Hryciw, M. L. Brongersma and M. D. McGehee, *J. Appl. Phys.*, 2009, **105**, 124509.
43. B. Weintraub, Y. Wei and Z. L. Wang, *Angew. Chem.*, 2009, **121**, 9143-9147.
44. A. L. Briseno, T. W. Holcombe, A. I. Boukai, E. C. Garnett, S. W. Shelton, J. J. Frechet and P. Yang, *Nano Lett.*, 2010, **10**, 334-340.
45. Y. J. Hwang, A. Boukai and P. Yang, *Nano Lett.*, 2009, **9**, 410-415.
46. M. T. Mayer, Y. Lin, G. Yuan and D. Wang, *Accounts of Chemical Research*, 2013.
47. J. Merten, J. M. Asensi, C. Voz, A. V. Shah, R. Platz and J. Andreu, *Electron Devices, IEEE Transactions on*, 1998, **45**, 423-429.
48. K. Nishioka, N. Sakitani, Y. Uraoka and T. Fuyuki, *Sol. Energy Mater. Sol. Cells*, 2007, **91**, 1222-1227.
49. M. A. Green, *Solid-State Electronics*, 1977, **20**, 265-266.
50. M. A. Green, *Solid-State Electronics*, 1981, **24**, 788-789.
51. C. Xiang, A. C. Meng and N. S. Lewis, *Proceedings of the National Academy of Sciences*, 2012, **109**, 15622-15627.
52. P. Yang, R. Yan and M. Fardy, *Nano Letters*, 2010, **10**, 1529-1536.
53. J. D. Christesen, X. Zhang, C. W. Pinion, T. A. Celano, C. J. Flynn and J. F. Cahoon, *Nano Lett.*, 2012, **12**, 6024-6029.

54. B. Tian, X. Zheng, T. J. Kempa, Y. Fang, N. Yu, G. Yu, J. Huang and C. M. Lieber, *Nature*, 2007, **449**, 885-889.
55. T. J. Kempa, J. F. Cahoon, S.-K. Kim, R. W. Day, D. C. Bell, H.-G. Park and C. M. Lieber, *Proceedings of the National Academy of Sciences*, 2012, **109**, 1407-1412.
56. M. A. Green, K. Emery, Y. Hishikawa, W. Warta and E. D. Dunlop, *Prog. Photovoltaics: Res. Appl.*, 2012, **20**, 606-614.
57. C. Colombo, M. Hei β , M. Grätzel and A. Fontcuberta i Morral, *Appl. Phys. Lett.*, 2009, **94**, 173108.
58. P. Krogstrup, H. I. Jorgensen, M. Heiss, O. Demichel, J. V. Holm, M. Aagesen, J. Nygard and A. Fontcuberta i Morral, *Nat Photon*, 2013, **7**, 306-310.
59. Y. Dong, B. Tian, T. J. Kempa and C. M. Lieber, *Nano Lett.*, 2009, **9**, 2183-2187.
60. J. M. Foley, M. J. Price, J. I. Feldblyum and S. Maldonado, *Energy & Environmental Science*, 2012, **5**, 5203-5220.
61. G. Yuan, K. Aruda, S. Zhou, A. Levine, J. Xie and D. Wang, *Angewandte Chemie International Edition*, 2011, **50**, 2334-2338.
62. R. Liu, C. Stephani, J. J. Han, K. L. Tan and D. Wang, *Angewandte Chemie International Edition*, 2013, **52**, 4225-4228.
63. B. Klahr, S. Gimenez, F. Fabregat-Santiago, T. Hamann and J. Bisquert, *Journal of the American Chemical Society*, 2012, **134**, 4294-4302.
64. F. Le Formal, N. Tetreault, M. Cornuz, T. Moehl, M. Gratzel and K. Sivula, *Chemical Science*, 2011, **2**, 737-743.
65. A. J. Bard, A. B. Bocarsly, F. R. F. Fan, E. G. Walton and M. S. Wrighton, *Journal of the American Chemical Society*, 1980, **102**, 3671-3677.
66. Y. J. Hwang, C. Hahn, B. Liu and P. Yang, *ACS Nano*, 2012, **6**, 5060-5069.
67. M. T. Mayer, C. Du and D. Wang, *J Am Chem Soc*, 2012, **134**, 12406-12409.
68. Y. J. Hwang, A. Boukai and P. Yang, *Nano Letters*, 2008, **9**, 410-415.
69. J. Q. Xi, M. F. Schubert, J. K. Kim, E. F. Schubert, M. Chen, S.-Y. Lin, LiuW and J. A. Smart, *Nat Photon*, 2007, **1**, 176-179.
70. Y. F. Huang, S. Chattopadhyay, Y. J. Jen, C. Y. Peng, T. A. Liu, Y. K. Hsu, C. L. Pan, H. C. Lo, C. H. Hsu, Y. H. Chang, C. S. Lee, K. H. Chen and L. C. Chen, *Nature Nanotech.*, 2007, **2**, 770-774.
71. B. C. P. Sturmberg, K. B. Dossou, L. C. Botten, A. A. Asatryan, C. G. Poulton, C. M. de Sterke and R. C. McPhedran, *Opt. Express*, 2011, **19**, A1067-A1081.
72. J. Wallentin, N. Anttu, D. Asoli, M. Huffman, I. Åberg, M. H. Magnusson, G. Siefer, P. Fuss-Kailuweit, F. Dimroth, B. Witzigmann, H. Q. Xu, L. Samuelson, K. Deppert and M. T. Borgström, *Science*, 2013, **339**, 1057-1060.
73. Z. Yu, A. Raman and S. Fan, *Proceedings of the National Academy of Sciences*, 2010, **107**, 17491-17496.
74. J. Kupec, R. L. Stoop and B. Witzigmann, *Opt. Express*, 2010, **18**, 27589-27605.
75. C. Lin and M. L. Povinelli, *Opt. Express*, 2009, **17**, 19371-19381.
76. M. D. Kelzenberg, S. W. Boettcher, J. A. Petykiewicz, D. B. Turner-Evans, M. C. Putnam, E. L. Warren, J. M. Spurgeon, R. M. Briggs, N. S. Lewis and H. A. Atwater, *Nature Mater.*, 2010, **9**, 239-244.
77. E. Garnett and P. Yang, *Nano Lett.*, 2010, **10**, 1082-1087.

78. Y. Lu and A. Lal, *Nano Lett.*, 2010, **10**, 4651-4656.
79. R. R. King, D. Bhusari, D. Larrabee, X. Q. Liu, E. Rehder, K. Edmondson, H. Cotal, R. K. Jones, J. H. Ermer, C. M. Fetzer, D. C. Law and N. H. Karam, *Prog. Photovoltaics: Res. Appl.*, 2012, **20**, 801-815.
80. *Foundations for Innovation: Photovoltaic Technologies for the 21st Century*, Steering Committee for Advancing Photovoltaic Technologies, 2010.
81. C. A. Wolden, J. Kurtin, J. B. Baxter, I. Repins, S. E. Shaheen, J. T. Torvik, A. A. Rockett, V. M. Fthenakis and E. S. Aydil, *Journal of Vacuum Science & Technology A: Vacuum, Surfaces, and Films*, 2011, **29**, 030801.
82. C. Marichy, M. Bechelany and N. Pinna, *Adv. Mater.*, 2012, **24**, 1017-1032.
83. Y. W. Chen, J. D. Prange, S. Dühnen, Y. Park, M. Gunji, C. E. D. Chidsey and P. C. McIntyre, *Nat Mater*, 2011, **10**, 539-544.
84. N. P. Dasgupta, C. Liu, S. Andrews, F. B. Prinz and P. Yang, *J. Am. Chem. Soc.*, 2013.
85. Z. Fan, H. Razavi, J.-w. Do, A. Moriwaki, O. Ergen, Y.-L. Chueh, P. W. Leu, J. C. Ho, T. Takahashi, L. A. Reichertz, S. Neale, K. Yu, M. Wu, J. W. Ager and A. Javey, *Nat Mater*, 2009, **8**, 648-653.
86. A. W. Snyder and J. D. Love, *Optical Waveguide Theory*, Chapman and Hall, New York, 1983.
87. K. Seo, M. Wober, P. Steinvurzel, E. Schonbrun, Y. Dan, T. Ellenbogen and K. B. Crozier, *Nano Lett.*, 2011, **11**, 1851-1856.
88. L. Cao, J. S. White, J. S. Park, J. A. Schuller, B. M. Clemens and M. L. Brongersma, *Nature Mater.*, 2009, **8**, 643-647.
89. G. Brönstrup, N. Jahr, C. Leiterer, A. Csáki, W. Fritzsche and S. Christiansen, *ACS Nano*, 2010, **4**, 7113-7122.
90. S. Brittman, H. Gao, E. C. Garnett and P. Yang, *Nano Lett.*, 2011, **11**, 5189-5195.
91. Y. Zhan, X. Li and Y. Li, *Selected Topics in Quantum Electronics, IEEE Journal of*, 2013, **PP**, 1-1.
92. J. W. Elam, N. P. Dasgupta and F. B. Prinz, *MRS Bulletin*, 2011, **36**, 899-906
M893 - 810.1557/mrs.2011.1265.
93. A. Paracchino, V. Laporte, K. Sivula, M. Grätzel and E. Thimsen, *Nat Mater*, 2011, **10**, 456-461.
94. B. A. Pinaud, J. D. Benck, L. C. Seitz, A. J. Forman, Z. Chen, T. G. Deutsch, B. D. James, K. N. Baum, G. N. Baum, S. Ardo, H. Wang, E. Miller and T. F. Jaramillo, *Energy & Environmental Science*, 2013.
95. S. Haussener, S. Hu, C. Xiang, A. Z. Weber and N. Lewis, *Energy & Environmental Science*, 2013.
96. J. O. M. Bockris, I. A. Ammar and A. K. M. S. Huq, *The Journal of Physical Chemistry*, 1957, **61**, 879-886.
97. N. M. Marković, B. N. Grgur and P. N. Ross, *The Journal of Physical Chemistry B*, 1997, **101**, 5405-5413.
98. J. R. McKone, E. L. Warren, M. J. Bierman, S. W. Boettcher, B. S. Brunschwig, N. S. Lewis and H. B. Gray, *Energy & Environmental Science*, 2011, **4**, 3573.

99. A. W. Jeremiasse, J. Bergsma, J. M. Kleijn, M. Saakes, C. J. N. Buisman, M. Cohen Stuart and H. V. M. Hamelers, *International Journal of Hydrogen Energy*, 2011, **36**, 10482-10489.
100. J. D. Benck, Z. Chen, L. Y. Kuritzky, A. J. Forman and T. F. Jaramillo, *ACS Catalysis*, 2012, **2**, 1916-1923.
101. J. Kibsgaard, Z. Chen, B. N. Reinecke and T. F. Jaramillo, *Nat Mater*, 2012, **11**, 963-969.
102. L. D. Burke, O. J. Murphy, J. F. O'Neill and S. Venkatesan, *Journal of the Chemical Society, Faraday Transactions 1: Physical Chemistry in Condensed Phases*, 1977, **73**, 1659-1671.
103. Y. Lee, J. Suntivich, K. J. May, E. E. Perry and Y. Shao-Horn, *The Journal of Physical Chemistry Letters*, 2012, **3**, 399-404.
104. M. W. Kanan and D. G. Nocera, *Science*, 2008, **321**, 1072-1075.
105. M. Dincă, Y. Surendranath and D. G. Nocera, *Proceedings of the National Academy of Sciences*, 2010, **107**, 10337-10341.
106. L. Trotochaud, J. K. Ranney, K. N. Williams and S. W. Boettcher, *Journal of the American Chemical Society*, 2012, **134**, 17253-17261.
107. R. D. L. Smith, M. S. Prévot, R. D. Fagan, Z. Zhang, P. A. Sedach, M. K. J. Siu, S. Trudel and C. P. Berlinguette, *Science*, 2013, **340**, 60-63.
108. J. B. Gerken, J. Y. C. Chen, R. C. Massé, A. B. Powell and S. S. Stahl, *Angewandte Chemie International Edition*, 2012, **51**, 6676-6680.
109. K. P. Kuhl, E. R. Cave, D. N. Abram and T. F. Jaramillo, *Energy & Environmental Science*, 2012, **5**, 7050.
110. E. Barton Cole, P. S. Lakkaraju, D. M. Rampulla, A. J. Morris, E. Abelev and A. B. Bocarsly, *Journal of the American Chemical Society*, 2010, **132**, 11539-11551.
111. A. M. Appel, J. E. Bercaw, A. B. Bocarsly, H. Dobbek, D. L. DuBois, M. Dupuis, J. G. Ferry, E. Fujita, R. Hille, P. J. A. Kenis, C. A. Kerfeld, R. H. Morris, C. H. F. Peden, A. R. Portis, S. W. Ragsdale, T. B. Rauchfuss, J. N. H. Reek, L. C. Seefeldt, R. K. Thauer and G. L. Waldrop, *Chemical Reviews*, 2013.
112. I. S. Cho, Z. Chen, A. J. Forman, D. R. Kim, P. M. Rao, T. F. Jaramillo and X. Zheng, *Nano Letters*, 2011, **11**, 4978-4984.
113. J. R. McKone, E. L. Warren, M. J. Bierman, S. W. Boettcher, B. S. Brunschwig, N. S. Lewis and H. B. Gray, *Energy & Environmental Science*, 2011, **4**, 3573-3583.
114. E. L. Warren, J. R. McKone, H. A. Atwater, H. B. Gray and N. S. Lewis, *Energy & Environmental Science*, 2012.
115. Y. Ling, G. Wang, D. A. Wheeler, J. Z. Zhang and Y. Li, *Nano Letters*, 2011, **11**, 2119-2125.
116. L. Li, Y. Yu, F. Meng, Y. Tan, R. J. Hamers and S. Jin, *Nano Letters*, 2012, **12**, 724-731.
117. H. M. Chen, C. K. Chen, Y.-C. Chang, C.-W. Tsai, R.-S. Liu, S.-F. Hu, W.-S. Chang and K.-H. Chen, *Angewandte Chemie International Edition*, 2010, **49**, 5966-5969.
118. H. M. Chen, C. K. Chen, R.-S. Liu, C.-C. Wu, W.-S. Chang, K.-H. Chen, T.-S. Chan, J.-F. Lee and D. P. Tsai, *Advanced Energy Materials*, 2011, **1**, 742-747.
119. J. Su, X. Feng, J. D. Sloppy, L. Guo and C. A. Grimes, *Nano Letters*, 2010, **11**, 203-208.

120. P. M. Rao, I. S. Cho and X. Zheng, *Proceedings of the Combustion Institute*, 2013, **34**, 2187-2195.
121. J. Sun, C. Liu and P. Yang, *Journal of the American Chemical Society*, 2011, **133**, 19306-19309.
122. C. Liu, J. Sun, J. Tang and P. Yang, *Nano Letters*, 2012, **12**, 5407-5411.
123. D. Wang, A. Pierre, M. G. Kibria, K. Cui, X. Han, K. H. Bevan, H. Guo, S. Paradis, A.-R. Hakima and Z. Mi, *Nano Letters*, 2011, **11**, 2353-2357.
124. B. AlOtaibi, M. Harati, S. Fan, S. Zhao, H. P. T. Nguyen, M. G. Kibria and Z. Mi, *Nanotechnology*, 2013, **24**, 175401.
125. K.-Q. Peng, X. Wang, X.-L. Wu and S.-T. Lee, *Nano Letters*, 2009, **9**, 3704-3709.
126. S. W. Boettcher, J. M. Spurgeon, M. C. Putnam, E. L. Warren, D. B. Turner-Evans, M. D. Kelzenberg, J. R. Maiolo, H. A. Atwater and N. S. Lewis, *Science*, 2010, **327**, 185-187.
127. S. W. Boettcher, E. L. Warren, M. C. Putnam, E. A. Santori, D. Turner-Evans, M. D. Kelzenberg, M. G. Walter, J. R. McKone, B. S. Brunschwig, H. A. Atwater and N. S. Lewis, *Journal of the American Chemical Society*, 2011, **133**, 1216-1219.
128. G. Yuan, H. Zhao, X. Liu, Z. S. Hasanali, Y. Zou, A. Levine and D. Wang, *Angewandte Chemie International Edition*, 2009, **48**, 9680-9684.
129. R. Liu, G. Yuan, C. L. Joe, T. E. Lightburn, K. L. Tan and D. Wang, *Angewandte Chemie International Edition*, 2012, **51**, 6537-6537.
130. Y. Hou, B. L. Abrams, P. C. K. Vesborg, M. E. Björketun, K. Herbst, L. Bech, A. M. Setti, C. D. Damsgaard, T. Pedersen, O. Hansen, J. Rossmeisl, S. Dahl, J. K. Nørskov and I. Chorkendorff, *Nat Mater*, 2011, **10**, 434-438.
131. C. Liu, Y. J. Hwang, H. E. Jeong and P. Yang, *Nano Letters*, 2011, **11**, 3755-3758.
132. J. Z. Zhang, *MRS Bulletin*, 2011, **36**, 48-55.
133. B. Seger, T. Pedersen, A. B. Laursen, P. C. K. Vesborg, O. Hansen and I. Chorkendorff, *Journal of the American Chemical Society*, 2013, **135**, 1057-1064.
134. M. H. Lee, K. Takei, J. Zhang, R. Kapadia, M. Zheng, Y.-Z. Chen, J. Nah, T. S. Matthews, Y.-L. Chueh, J. W. Ager and A. Javey, *Angewandte Chemie International Edition*, 2012, **51**, 10760-10764.
135. J. K. Kurdett, *Chemical Bonding in Solids*, Oxford University Press, 1995.
136. M. Law, L. E. Greene, J. C. Johnson, R. Saykally and P. Yang, *Nature Mater.*, 2005, **4**, 455-459.
137. X. Chen, C. Li, M. Gratzel, R. Kostecki and S. S. Mao, *Chem. Soc. Rev.*, 2012, **41**, 7909-7937.
138. S. Ito, S. M. Zakeeruddin, R. Humphry-Baker, P. Liska, R. Charvet, P. Comte, M. K. Nazeeruddin, P. Péchy, M. Takata, H. Miura, S. Uchida and M. Grätzel, *Adv. Mater.*, 2006, **18**, 1202-1205.
139. L. E. Greene, M. Law, B. D. Yuhas and P. Yang, *The Journal of Physical Chemistry C*, 2007, **111**, 18451-18456.
140. T. C. Monson, M. T. Lloyd, D. C. Olson, Y.-J. Lee and J. W. P. Hsu, *Adv. Mater.*, 2008, **20**, 4755-4759.
141. Y.-Y. Lin, Y.-Y. Lee, L. Chang, J.-J. Wu and C.-W. Chen, *Appl. Phys. Lett.*, 2009, **94**, 063308.

142. B. D. Yuhas and P. Yang, *J. Am. Chem. Soc.*, 2009, **131**, 3756-3761.
143. A. I. Hochbaum, R. Chen, R. D. Delgado, W. Liang, E. C. Garnett, M. Najarian, A. Majumdar and P. Yang, *Nature*, 2008, **451**, 163-167.
144. E. C. Garnett and P. Yang, *J. Am. Chem. Soc.*, 2008, **130**, 9224-9225.
145. I. Zoric, M. Zäch, B. Kasemo and C. Langhammer, *ACS Nano*, 2011, **5**, 2535-2546.
146. S. A. Maier and H. A. Atwater, *J. Appl. Phys.*, 2005, **98**, 011101.
147. C. Langhammer, M. Schwind, B. Kasemo and I. Zoric, *Nano Lett.*, 2008, **8**, 1461-1471.
148. K. L. Kelly, E. Coronado, L. L. Zhao and G. C. Schatz, *J. Phys. Chem. B*, 2003, **107**, 668-677.
149. C. F. Bohren and D. R. Huffman, *Absorption and Scattering of Light by Small Particles*, John Wiley & Sons, New York, 1983.
150. E. Hao and G. C. Schatz, *J. Chem. Phys.*, 2004, **120**, 357-366.
151. H. A. Atwater and A. Polman, *Nature Mater.*, 2010, **9**, 205-213.
152. A. P. Kulkarni, K. M. Noone, K. Munechika, S. R. Guyer and D. S. Ginger, *Nano Lett.*, 2010, **10**, 1501-1505.
153. K. R. Catchpole and A. Polman, *Appl. Phys. Lett.*, 2008, **93**, 191113.
154. H. Gao, C. Liu, H. E. Jeong and P. Yang, *ACS Nano*, 2011, **6**, 234-240.
155. J. H. Kennedy and K. W. Frese, *J. Electrochem. Soc.*, 1978, **125**, 709-714.
156. T. Kuykendall, P. J. Pauzauskie, Y. Zhang, J. Goldberger, D. Sirbuly, J. Denlinger and P. Yang, *Nat Mater*, 2004, **3**, 524-528.
157. Y. J. Hwang, C. H. Wu, C. Hahn, H. E. Jeong and P. Yang, *Nano Letters*, 2012, **12**, 1678-1682.

Figure Captions

Figure X.1: Principles of solar cells. a) Schematic and energy band diagram of a *p-n* homojunction that produces the built-in electric field used to separate photogenerated charges in a solar cell. b) The AM 1.5G solar spectrum from 300-1500 nm. c) *I-V* characteristic of a solar cell in the dark and light showing the metrics for quantifying its performance.

Figure X.2: Principles of photoelectrochemical cells. a) Energy diagram of the electric field (band-bending) at the semiconductor/electrolyte interface. b) When the circuit is closed by a metal counter electrode, the illuminated junction produces a net current flow. c) The "Z-scheme" uses two semiconductors of different band gaps to perform the redox reactions that store the energy of absorbed photons in chemical fuels. At each electrode, the photogenerated minority carriers react at the surface, while the majority carriers recombine at the interface connecting the two electrodes.

Figure X.3: Benefits of the nanowire geometry for charge collection. a) In a nanowire's radial *p-n* junction, photogenerated carriers travel only a short distance to be separated by the built-in electric field. b) Nanowire arrays orthogonalize the directions of light absorption (axial) and charge separation (radial), facilitating the use of materials whose optical absorption lengths significantly exceed their minority carrier diffusion lengths. Nanowire arrays can also provide in-plane light-trapping effects because of scattering and optical modes that arise from the interactions among the nanowires. The length scales given are approximate and will depend upon the material properties of the semiconductor.

Figure X.4: Equivalent circuit models of PV and PEC cells. a) Diagrams and corresponding equations for ideal and practical devices. Only a single diode is shown, representing the drift-diffusion current, although others can be added to model additional transport processes. Illumination of the cells produces a current (I_L) that opposes the diode's current and gives rise to a photogenerated voltage (V). Various resistances (R_{series} and R_{shunt}) reduce the efficiency of the cells. In the PEC cell, the circuit's chemical reaction is modeled by the Butler-Volmer equation and causes an overpotential (η)-dependent series resistance ($R_{B\text{-}V}$). The high surface area of the TiO_2 nanorods (NRs) and branched nanorods (B-NRs) shown schematically and in scanning electron microscopy (SEM) images (b) allows more current to be generated at the same overpotential, dramatically improving the fill factor of the photocurrent curve (c). Additionally, the nanorods also benefit from increased light absorption and improved charge transport as compared to the nanoparticle film (NPs). Because the light absorption of the NRs and B-NRs is similar (not shown), the enhanced IPCE of the B-NRs (d) suggests that their increased surface area reduces the overpotential-dependent series resistance and therefore improves charge collection at the surface. Figures b-d are adapted with permission from reference 112. Copyright 2011, American Chemical Society.

Figure X.5: A 13.8%- efficient nanowire array solar cell. a) Top-view and tilted-view (inset) SEM images of an array of InP nanowires used to form the most efficient nanowire array solar cell to date. b) Side-view SEM and schematic of the completed solar cell. Note that the junction is axial rather than radial, implying that this device does not take advantage of a nanowire array's ability to orthogonalize the directions of light absorption and charge separation. c) Current density-voltage (*J*-*V*) curve of the record nanowire InP solar cell, normalized to the device's entire unmetallized cross-sectional area, including gaps between the wires. This figure is adapted with permission from reference 72. Copyright 2013, American Association for the Advancement of Science.

Figure X.6: Optical properties of individual semiconductor nanowires. a) Numerical simulations showing the theoretical maximum photocurrent density in nanowires under one-sun, AM 1.5 illumination based on their diameter and cross-sectional geometry (inset). Trends are similar for different cross-sections, and photocurrent densities far exceed those produced in a thin film of equivalent volume. b) The spectral dependence of the nanowires' absorption efficiency at the second enhancement peak in (a) near 130 nm (180 nm for the triangular wire). c) Plots of the electric field intensity of the mode near 700 nm in (b) in nanowires of differing cross-sections, showing that the mode profile is similar for all cross-sections. In a-c, the optical properties of amorphous silicon were used. Figures a-c are reprinted with permission from reference 14. Copyright 2010, American Chemical Society. d) Experimental and numerical simulations of the EQE of two different silicon single-nanowire solar cells, normalized to their geometrical cross-sections. The experiments match well with the simulated results, and both show that the nanowire's absorption cross-section can exceed its geometrical cross-section, which appears as an EQE exceeding unity. The nanowires absorb much more strongly than a planar film of equivalent thickness. Figure d is adapted with permission from reference 55. Copyright 2012, National Academy of Sciences.

Figure X.7: Matching charge flux densities between electrocatalysts and light absorbers. The required overpotential (η) to reach 10 mA/cm^2 (the threshold of commercial relevance) is plotted versus the exchange current density (i_0) of a planar electrode loaded with various catalysts. The percentage of voltage lost, relative to the 1.23V required thermodynamically to split water, is also shown (right y-axis). The dashed blue curve is a calculation for 100% surface coverage of the catalyst, assuming a 59 mV/decade Tafel slope in the Butler-Volmer equation, while the yellow curve assumes only 10% surface coverage. Pt,[96,97] NiMo,[98,99] and MoS_x[100,101]are catalysts for hydrogen evolution, while IrO_x/RuO_x,[102,103] CoPi and its derivatives,[104,105] and amorphous NiCoFe oxide[106-108] are catalysts for oxygen evolution. (The overpotential required to achieve 10 mA/cm^2 using catalysts for CO_2 reduction exceeds the values in this plot.[109-111]) The solid red curve indicates that a nanowire electrode with a roughness factor of 1000 and 10% catalyst coverage can significantly reduce the overpotential required to achieve the target current density. It should be noted that the catalytic activities listed here are intended to be planar monolayers for fair comparison and fundamental analysis; however, this information is not available for every electrocatalyst under 10 mA/cm^2, so some extrapolation and approximations were made. Detailed information about individual catalysts can be found in the references.

Figure X.8: Theoretical photocurrent densities for semiconductors under one-sun illumination. Based on integration of the one-sun, AM1.5G solar spectrum, maximum photocurrent densities for bulk semiconductors of interest in solar energy conversion are plotted versus their band gaps. Arrows at the bottom indicate the ultraviolet (below 400 nm), visible (400-750 nm), and infrared (beyond 750 nm) regions of the spectrum.

Figure X.9: A dye-sensitized solar cell (DSSC) based on ZnO nanowires.[136] a) Schematic of the design of the DSSC. b) SEM image of the ZnO nanowire array. Scale bar is 5 µm. c) *J-V* curves of two DSSCs under simulated one-sun, AM1.5G illumination, one with 0.8 cm^2 active area and the other with 0.2 cm^2 area. The EQE of the larger cell peaks near the dye's maximum absorption (inset).

Figure X.10: CdS/Cu_2S single-nanowire solar cells.[37] a) High-resolution TEM image of the high-quality interface between the CdS nanowire and its Cu_2S shell produced by a cation-exchange reaction. b) A reconstructed image of the square shown in (b) produced from the inverse fast Fourier transform (FFT) of diffraction spots from the nanowire's growth direction. Most of the lattice planes are continuous across the interface, although a distortion is highlighted in green. c) *I-V* characteristic of a single-nanowire solar cell showing a V_{oc} and *FF* that exceed those of planar CdS/Cu_2S solar cells.

Figure X.11: Silicon nanowire array solar cells.[77] a) Tilted cross-sectional SEM image of the silicon nanowire array produced by top-down etching. Scale bar is 1 µm. b) Optical image of the large-scale periodicity of the nanowires that make up 36 array solar cells.

Scale bar is 4 cm. c) Optical transmission of the films of etched silicon nanowires showing their reduced transmission at long wavelengths, which suggests that significant light trapping occurs within the nanowire films. d) Metrics of the radial *p-n* junction silicon nanowire array solar cells demonstrate that increasing the length of the nanowires (their roughness factor) increases their photocurrent and especially their photocurrent normalized to the volume of material present. V_{oc} and FF significantly decrease, however, because of increased recombination and dilution of the incident light across a larger junction area.

Figure X.12: Plasmonic nanostructures for solar energy conversion.[154,90] a) Gold nanorods coated with hematite (Fe_2O_3) produced larger photoanodic current than the planar control because of their enhanced light absorption. b) The enhancements correspond well with the simulated plasmonic resonances of the gold nanorods near 624 and 681 nm (simulation not shown). c) Side-view SEM image of a silver octahedral nanocrystal (inset) suspended from a silicon single-nanowire solar cell, a system designed to investigate the interactions between plasmonic and dielectric nanostructures. d) Numerical simulations of the electric field distribution within the wire-nanocrystal system indicate that the wavelength-dependent changes in the solar cell's photocurrent arise from increased absorption at the nanocrystal's plasmonic resonances (e.g. 750 nm and 981 nm) and reduced absorption when the nanocrystal locally disrupts one of the wire's own optical resonances (e.g. 661 nm).

Figure X.13: Solution-processed GaP nanowires for PEC.[122] a) A one-liter bottle of surfactant-free, SLS-grown GaP nanowires, demonstrating the scalability of this synthetic technique. b) TEM image of the SLS-grown GaP nanowires. c) The photocurrent and photovoltage of the GaP nanowire photocathode can be tuned and optimized by doping the wires with Zn during their synthesis. The photocurrent is normalized to that of a planar GaP photocathode operated under the same conditions, showing that because of its high surface area and more efficient charge collection, a very thin layer of solution-processed nanowires can produce photocurrent similar to that of a bulk electrode.

Figure X.14: Ultra-low loading of electrocatalytic Pt using ALD.[84] a) A scanning TEM high-angle annular dark-field (STEM-HAADF) image showing that ALD can coat high-aspect-ratio nanowires uniformly with sub-monolayer electrocatalysts. Here 10 cycles of ALD Pt was deposited onto a Si/TiO_2 core-shell nanowire. b) PEC performance of a Si/TiO_2 nanowire photocathode with increasing amounts of Pt loaded by ALD ranging from 1-10 cycles. 1 cycle corresponds to approximately 2.7% of a monolayer of surface coverage.

Figure X.15: "Z-scheme" artificial photosynthesis using an integrated system of nanostructures.[131,26] a) SEM image of the Si/TiO_2 asymmetric core-shell nanowires used to investigate the "Z-scheme" dynamics pictured energetically in (b) and detected by the UV-light-induced change in surface potential using scanning Kelvin probe force microscopy (c). Upon illumination, photoexcited minority carriers move to the surface of the two materials, while majority carriers recombine at the Si/TiO_2 interface. d) This design was then further developed to produce Si/TiO_2 nanotrees for solar water-splitting. e) A false-color SEM image of the nanotrees shows the dense TiO_2 nanowires designed to match better the higher charge flux of the Si nanowire. f) These nanotrees perform unbiased solar water-splitting, producing a 2:1 ratio of hydrogen and oxygen.

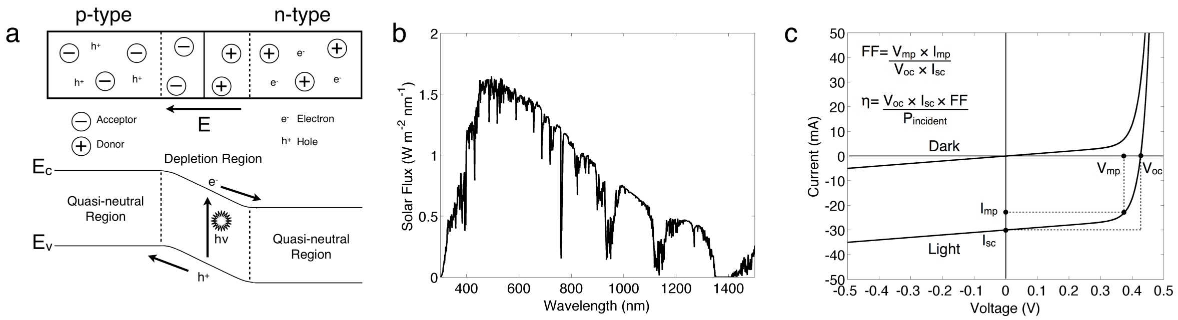
a
p-type
n-type
h+
e-
E
Acceptor
Donor
e- Electron
h+ Hole
Depletion Region
E_c
E_v
Quasi-neutral Region
Quasi-neutral Region
hν
b
Solar Flux (W m^{-2} nm^{-1})
0
0.5
1
1.5
2
400
600
800
1000
1200
1400
Wavelength (nm)
c
$FF = \frac{V_{mp} \times I_{mp}}{V_{oc} \times I_{sc}}$
$\eta = \frac{V_{oc} \times I_{sc} \times FF}{P_{incident}}$
Current (mA)
50
40
30
20
10
0
-10
-20
-30
-40
-50
-0.5
-0.4
-0.3
-0.2
-0.1
0
0.1
0.2
0.3
0.4
0.5
Voltage (V)
Dark
Light
V_{mp}
V_{oc}
I_{mp}
I_{sc}

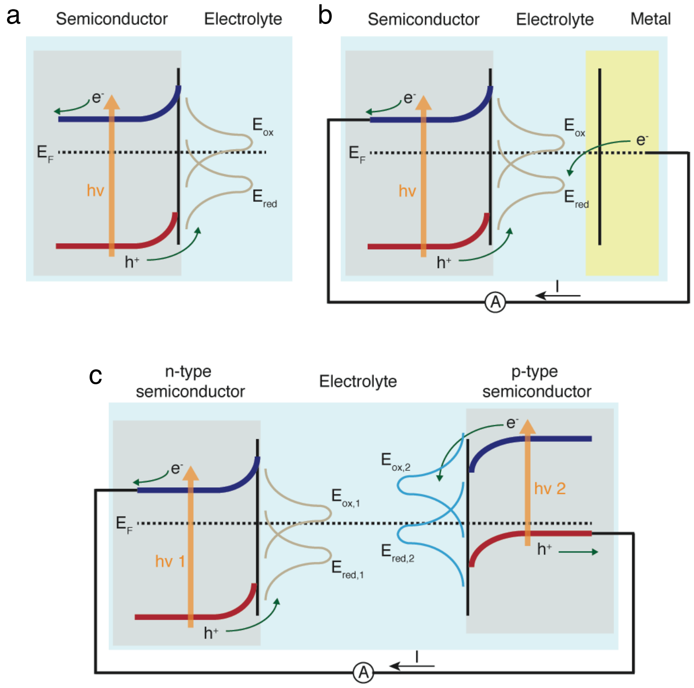
a
Semiconductor
Electrolyte
e-
E_{ox}
E_F
hv
E_{red}
h+
b
Semiconductor
Electrolyte
Metal
e-
E_{ox}
e-
E_F
hv
E_{red}
h+
I
A
c
n-type semiconductor
Electrolyte
p-type semiconductor
e-
$E_{ox,2}$
e-
$E_{ox,1}$
hv 2
E_F
hv 1
$E_{red,2}$
h+
$E_{red,1}$
h+
I
A

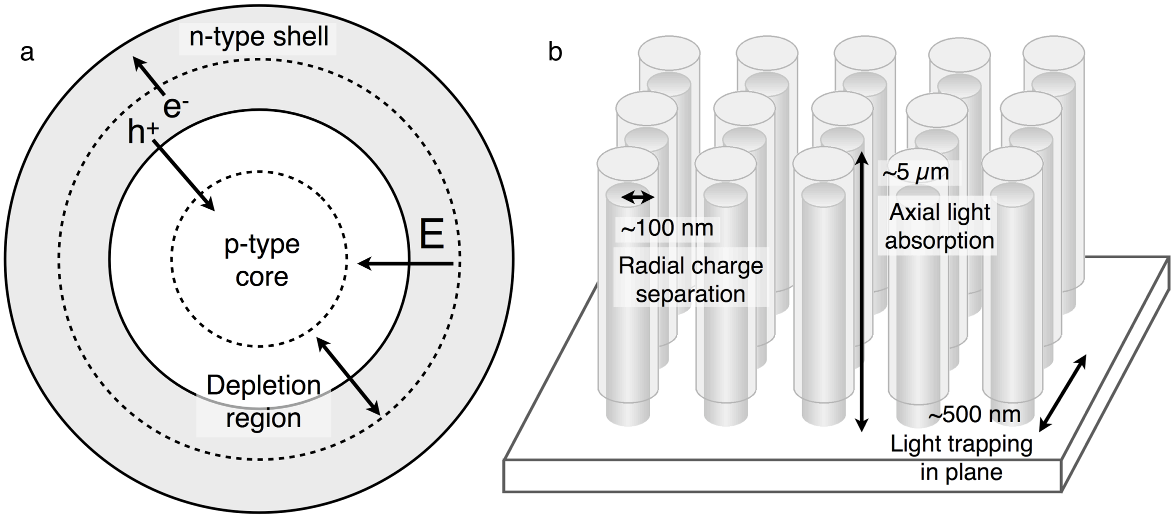
a
n-type shell
e-
h+
p-type core
E
Depletion region
b
~5 μm
~100 nm
Axial light absorption
Radial charge separation
~500 nm
Light trapping in plane

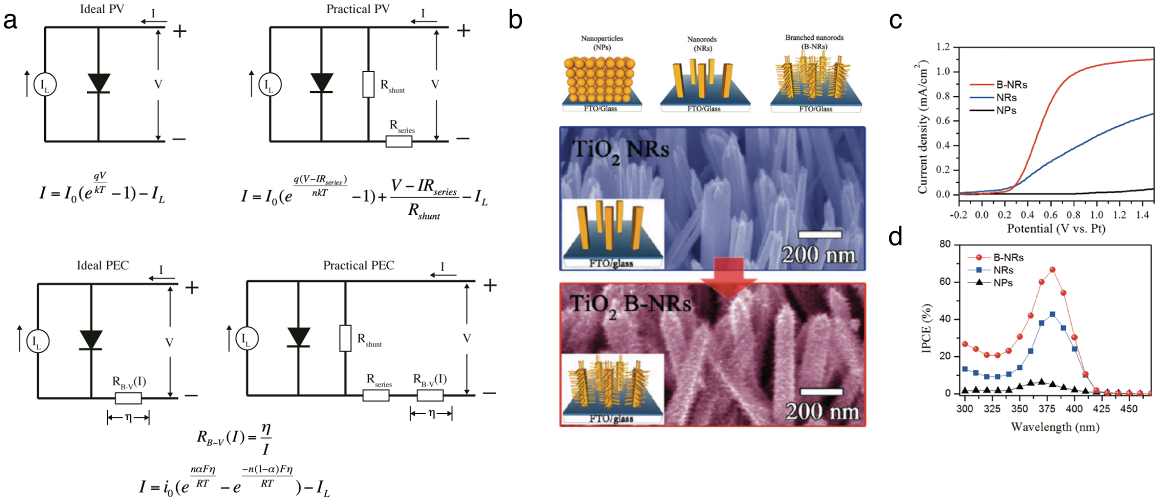
a
Ideal PV
Practical PV
Ideal PEC
Practical PEC
I
V
+
−
I_L
R_{shunt}
R_{series}
$R_{B-V}(I)$
η
$I = I_0(e^{\frac{qV}{kT}} - 1) - I_L$
$I = I_0(e^{\frac{q(V-IR_{series})}{nkT}} - 1) + \frac{V - IR_{series}}{R_{shunt}} - I_L$
$R_{B-V}(I) = \frac{\eta}{I}$
$I = i_0(e^{\frac{n\alpha F\eta}{RT}} - e^{\frac{-n(1-\alpha)F\eta}{RT}}) - I_L$
b
Nanoparticles (NPs)
Nanorods (NRs)
Branched nanorods (B-NRs)
FTO/Glass
TiO2 NRs
TiO2 B-NRs
FTO/glass
200 nm
c
Current density (mA/cm²)
Potential (V vs. Pt)
B-NRs
NRs
NPs
d
IPCE (%)
Wavelength (nm)

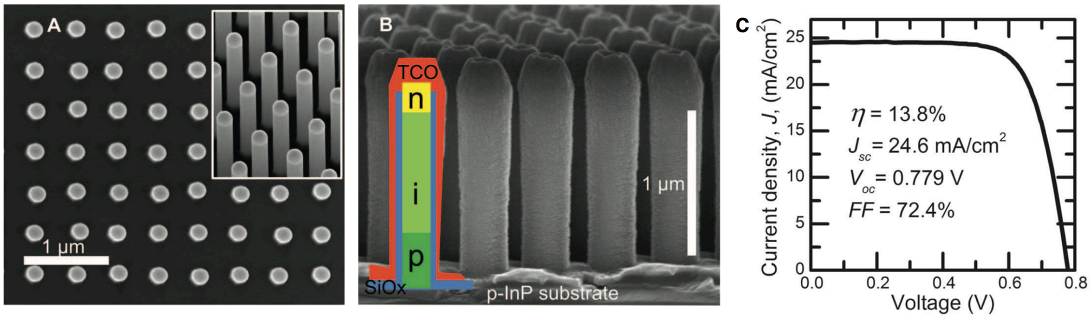
A
1 µm
B
TCO
n
i
p
SiOx
p-InP substrate
1 µm
c
Current density, J, (mA/cm²)
Voltage (V)
η = 13.8%
J_{sc} = 24.6 mA/cm²
V_{oc} = 0.779 V
FF = 72.4%

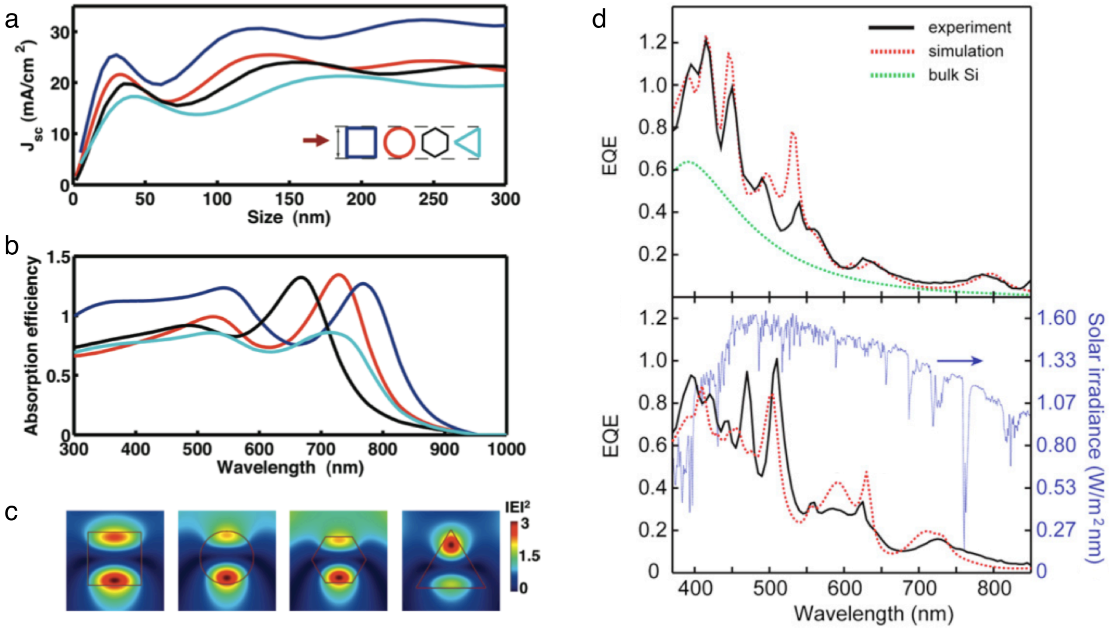
a
J_{sc} (mA/cm²)
Size (nm)
b
Absorption efficiency
Wavelength (nm)
c
|E|²
3
1.5
0
d
EQE
experiment
simulation
bulk Si
EQE
Solar irradiance (W/m²nm)
Wavelength (nm)

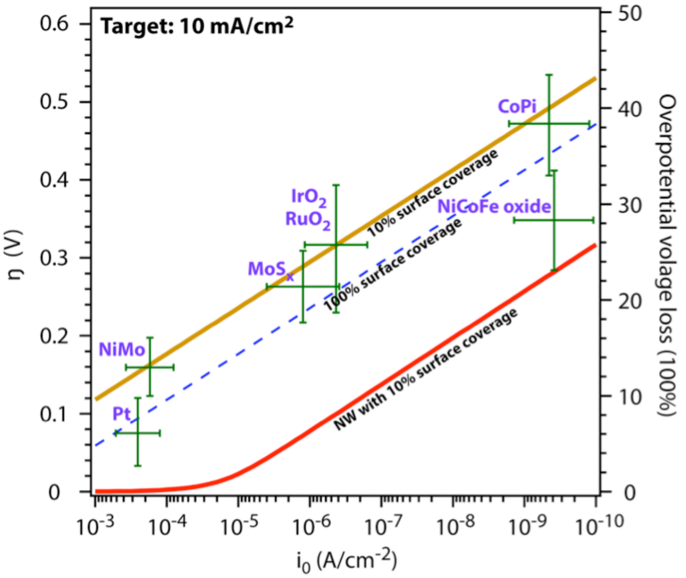
Target: 10 mA/cm²
η (V)
Overpotential volage loss (100%)
i_0 (A/cm^{-2})
10% surface coverage
100% surface coverage
NW with 10% surface coverage
CoPi
IrO_2
RuO_2
NiCoFe oxide
MoS_x
NiMo
Pt
0.6
0.5
0.4
0.3
0.2
0.1
0
50
40
30
20
10
0
10^{-3}
10^{-4}
10^{-5}
10^{-6}
10^{-7}
10^{-8}
10^{-9}
10^{-10}

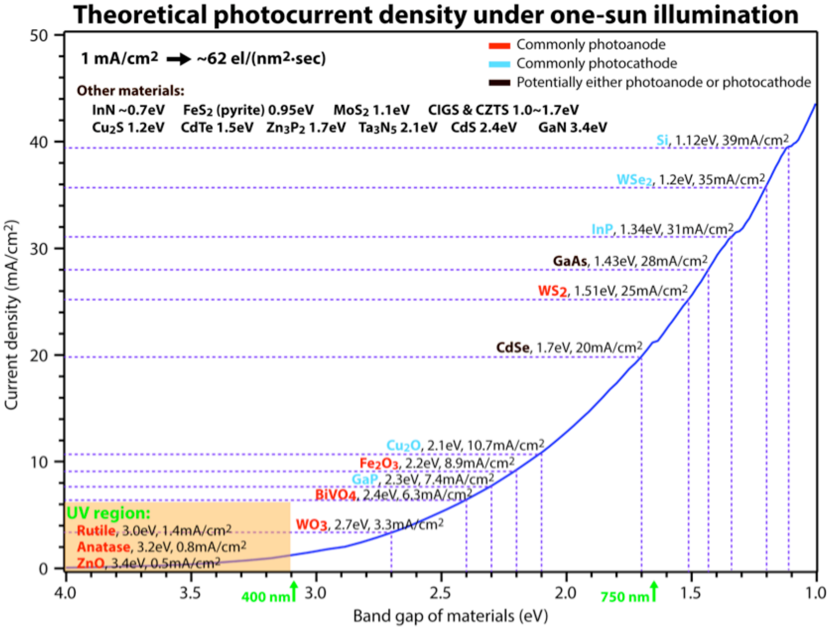
Theoretical photocurrent density under one-sun illumination
1 mA/cm² → ~62 el/(nm²·sec)
Commonly photoanode
Commonly photocathode
Potentially either photoanode or photocathode
Other materials:
InN ~0.7eV FeS₂ (pyrite) 0.95eV MoS₂ 1.1eV CIGS & CZTS 1.0~1.7eV
Cu₂S 1.2eV CdTe 1.5eV Zn₃P₂ 1.7eV Ta₃N₅ 2.1eV CdS 2.4eV GaN 3.4eV
Si, 1.12eV, 39mA/cm²
WSe₂, 1.2eV, 35mA/cm²
InP, 1.34eV, 31mA/cm²
GaAs, 1.43eV, 28mA/cm²
WS₂, 1.51eV, 25mA/cm²
CdSe, 1.7eV, 20mA/cm²
Cu₂O, 2.1eV, 10.7mA/cm²
Fe₂O₃, 2.2eV, 8.9mA/cm²
GaP, 2.3eV, 7.4mA/cm²
BiVO₄, 2.4eV, 6.3mA/cm²
WO₃, 2.7eV, 3.3mA/cm²
UV region:
Rutile, 3.0eV, 1.4mA/cm²
Anatase, 3.2eV, 0.8mA/cm²
ZnO, 3.4eV, 0.5mA/cm²
Current density (mA/cm²)
Band gap of materials (eV)
400 nm
750 nm
50
40
30
20
10
0
4.0
3.5
3.0
2.5
2.0
1.5
1.0

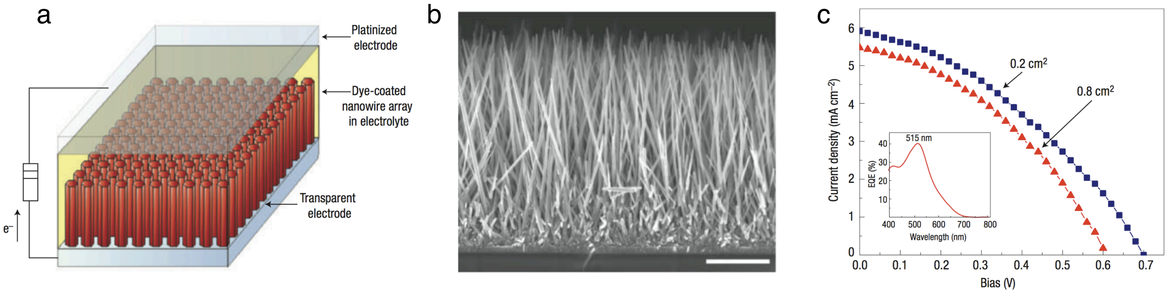
a
Platinized electrode
Dye-coated nanowire array in electrolyte
Transparent electrode
e⁻
b
c
0.2 cm²
0.8 cm²
515 nm
EQE (%)
Wavelength (nm)
400
500
600
700
800
40
30
20
10
Current density (mA cm⁻²)
Bias (V)
6
5
4
3
2
1
0
0.0
0.1
0.2
0.3
0.4
0.5
0.6
0.7

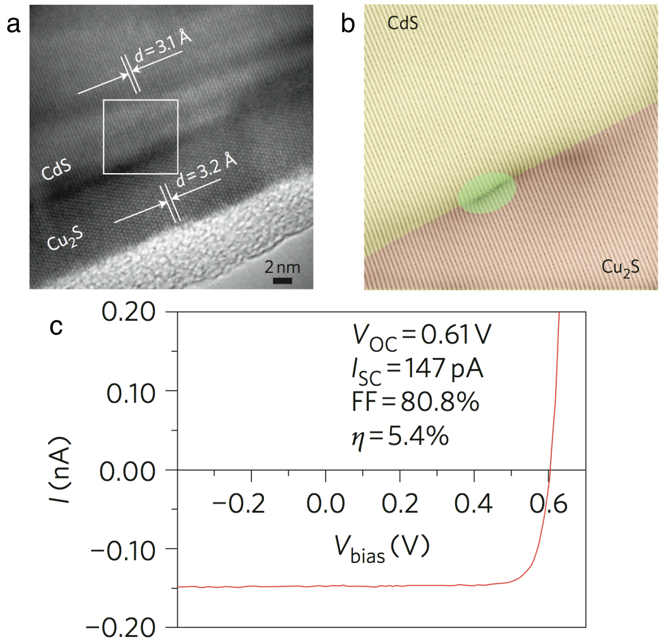
a
d = 3.1 Å
CdS
d = 3.2 Å
Cu$_2$S
2 nm
b
CdS
Cu$_2$S
c
V_{OC} = 0.61 V
I_{SC} = 147 pA
FF = 80.8%
η = 5.4%
0.20
0.10
0.00
−0.10
−0.20
I (nA)
−0.2
0.0
0.2
0.4
0.6
V_{bias} (V)

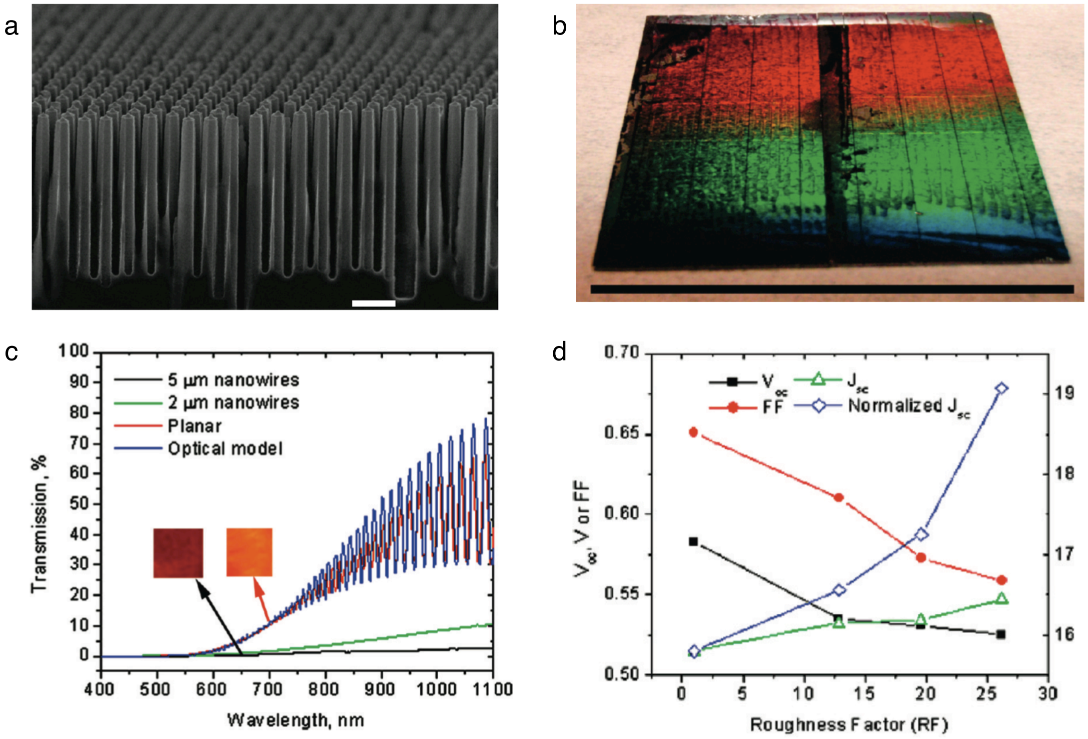
a
b
c
100
90
80
70
60
50
40
30
20
10
0
Transmission, %
5 µm nanowires
2 µm nanowires
Planar
Optical model
400
500
600
700
800
900
1000
1100
Wavelength, nm
d
0.70
0.65
0.60
0.55
0.50
V_{oc}, V or FF
V_{oc}
J_{sc}
FF
Normalized J_{sc}
19
18
17
16
0
5
10
15
20
25
30
Roughness Factor (RF)

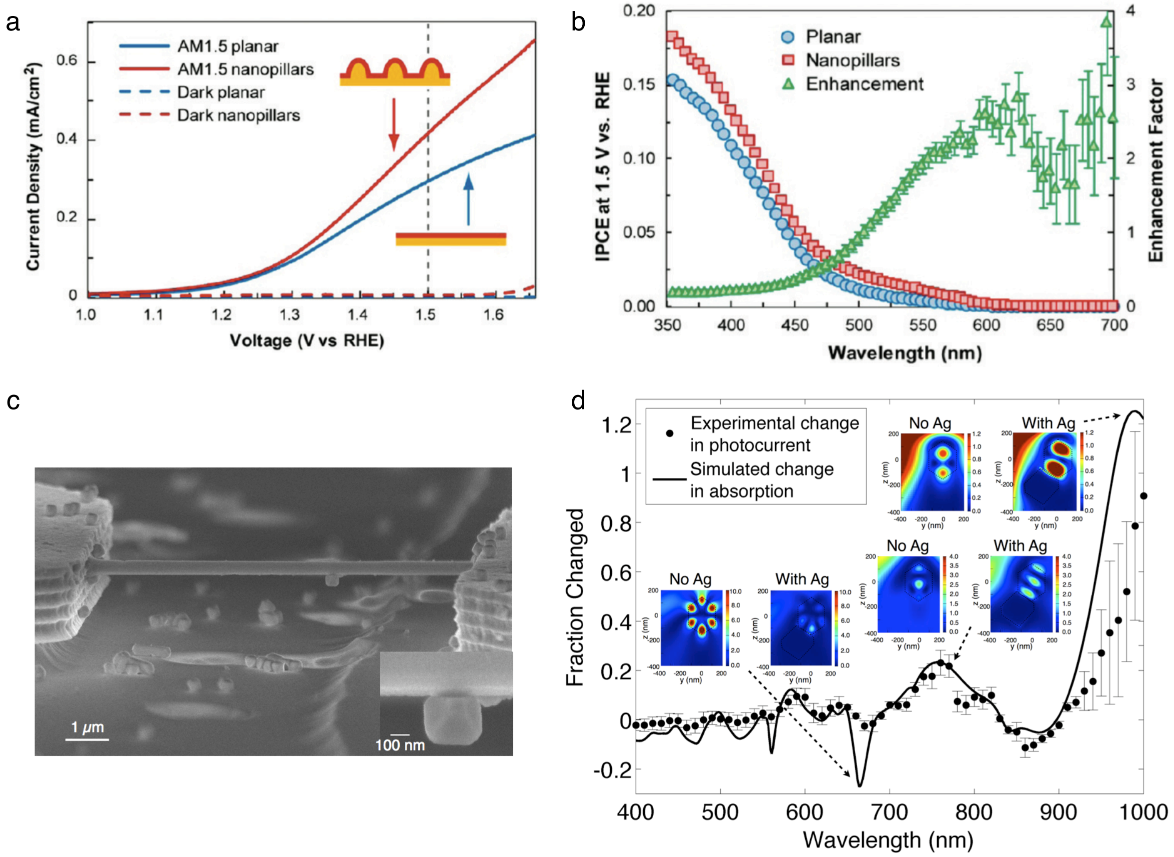
a
AM1.5 planar
AM1.5 nanopillars
Dark planar
Dark nanopillars
Current Density (mA/cm²)
Voltage (V vs RHE)
0
0.2
0.4
0.6
1.0
1.1
1.2
1.3
1.4
1.5
1.6
b
Planar
Nanopillars
Enhancement
IPCE at 1.5 V vs. RHE
Enhancement Factor
Wavelength (nm)
0.00
0.05
0.10
0.15
0.20
350
400
450
500
550
600
650
700
0
1
2
3
4
c
1 μm
100 nm
d
Experimental change in photocurrent
Simulated change in absorption
No Ag
With Ag
No Ag
With Ag
No Ag
With Ag
Fraction Changed
Wavelength (nm)
-0.2
0
0.2
0.4
0.6
0.8
1
1.2
400
500
600
700
800
900
1000

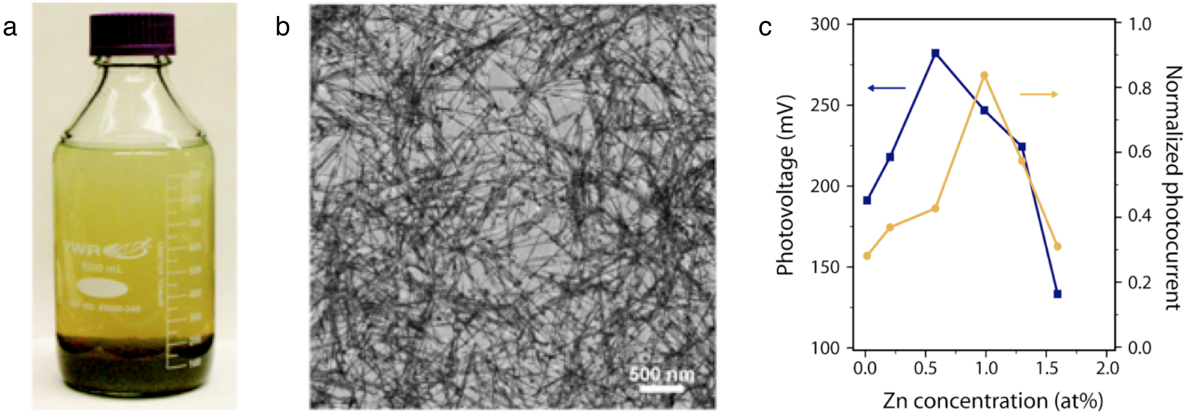
a
b
500 nm
c
Photovoltage (mV)
Normalized photocurrent
Zn concentration (at%)
100
150
200
250
300
0.0
0.2
0.4
0.6
0.8
1.0
0.0
0.5
1.0
1.5
2.0

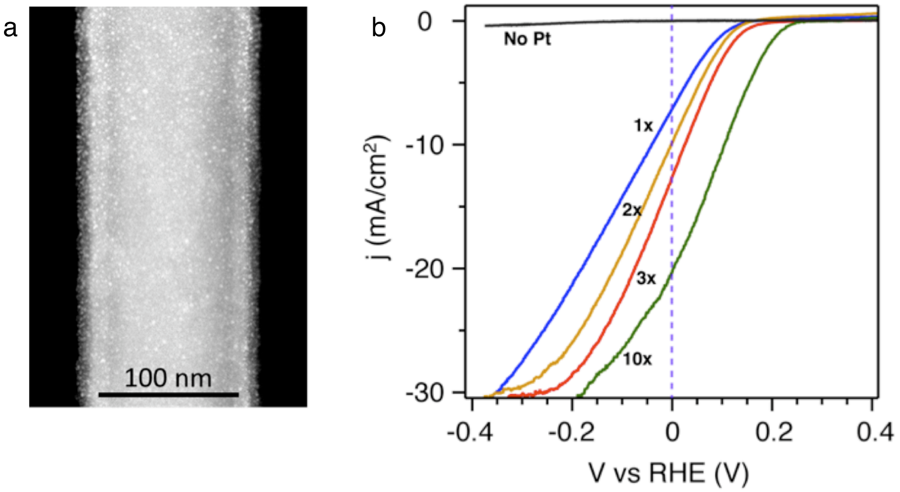
a
100 nm
b
No Pt
1x
2x
3x
10x
j (mA/cm²)
V vs RHE (V)
0
-10
-20
-30
-0.4
-0.2
0
0.2
0.4

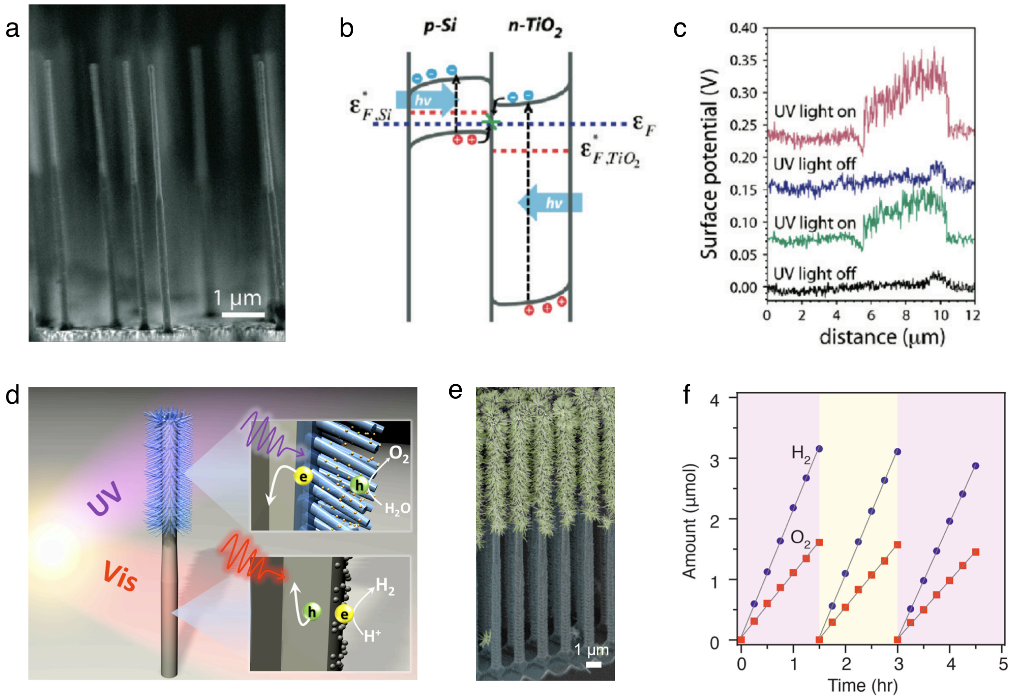
a
1 µm
b
p-Si
n-TiO$_2$
hν
$\varepsilon^*_{F,Si}$
ε_F
ε^*_{F,TiO_2}
hν
c
Surface potential (V)
0.40
0.35
0.30
0.25
0.20
0.15
0.10
0.05
0.00
UV light on
UV light off
UV light on
UV light off
0
2
4
6
8
10
12
distance (µm)
d
UV
Vis
e
h
O$_2$
H$_2$O
h
e
H$_2$
H$^+$
e
1 µm
f
Amount (µmol)
4
3
2
1
0
H$_2$
O$_2$
0
1
2
3
4
5
Time (hr)